Geochemistry 83 (2023) 125978

Contents lists available at ScienceDirect

Geochemistry

journal homepage: www.elsevier.com/locate/chemer

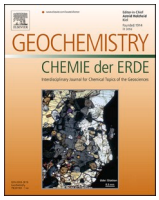

Mineralogical and geochemical characterization of lacustrine calcareous shale in Dongying Depression, Bohai Bay Basin: Implications for paleosalinity, paleoclimate, and paleoredox conditions

Danish Khan [a,b,*], Liu Zijun [c], Longwei Qiu [b,**], Liu Kuiyuan [c], Yang Yongqiang [b], Nie Cong [c], Liu Bin [c], Xin Li [b], Yerejiepu Habulashenmu [b]

[a] State Key Laboratory of Ore Deposit Geochemistry, Institute of Geochemistry, Chinese Academy of Sciences, Guiyang 550081, China
[b] School of Geosciences, China University of Petroleum, Qingdao 266000, China
[c] Hekou Oil Production Plant, SINOPEC Shengli Oilfield Company, Dongying 257000, China

ARTICLE INFO

Handling Editor: Priyadarsi D. Roy

Keywords:
Shale lithofacies
Paleosalinity
Paleoclimate
Depositional environment
Shahejie Formation
Bohai Bay Basin

ABSTRACT

Shale is an important self-sourced reservoir rock in many sedimentary basins worldwide. In this research work, a geochemical history of variations in the sedimentary environment of the lacustrine basin is analyzed based on extensive shale samples collected from the lower 3rd member (Es_3^L) and upper 4th member (Es_4^U) of the Paleogene Shahejie Formation in the Boxing Sag (Dongying Depression, East Coast of China). The representative shale samples were analyzed for total organic carbon (TOC) contents, mineralogical composition, the concentration of different elements (major, minor, and trace), kerogen types and vitrinite reflectance (R_o), and different sedimentary structures to understand the evolution of the depositional settings and their effect on the distribution of shale lithofacies in this basin. The TOC content in this shale ranges from 0.08 % to 13.6 %. R_o values range from 0.55 to 1.19 % with type-I to type-II kerogens. The studied shale is composed of calcite (average 37.83 wt%), dolomite (avg. 10.47 wt%), quartz (avg. 23.8 wt%), plagioclase (avg. 3.91 wt%), clay (avg. 20.84 wt%), and pyrite (avg. 2.85 wt%). Seven lithofacies have been established including mixed shale, calcareous shale, laminated limestone, argillaceous shale, dolomitic shale, siliceous shale, and siliceous dolomite based on mineral composition, TOC contents, and sedimentary structures. Different geochemical proxies including Sr/Ba, Ca/Ca + Fe, C-values, CIA values, Ti/Al, Al/Al + Fe, Al/Ti, *V*/V + Ni, Ni/Co, and Fe/Ca + Mg were used to interpret salinity, paleoclimate, detrital influx, provenance, paleoredox and water depth of the depositional environment in the studied shale. The detailed interpretation of the sedimentary environment suggested that during the deposition of Es_3^L shale, the terrigenous influx was high in shallow to a deep open lacustrine system with higher primary biogenic productivity. Semi-humid climatic conditions with higher precipitation rates prevailed during the deposition of this shale. On the other hand, relatively limited terrigenous input with low bioproductivity prevailed during the deposition of Es_4^U shale in the study area. Semiarid to humid climatic conditions with strong evaporation prevailed during the deposition of this shale. In this research work, a detailed depositional model of the Es_3^L–Es_4^U shale in Boxing Sag is established. The interpretations deduced from the current research work are likely to expand the knowledge of shale lithofacies and the genesis of lacustrine fine-grained sedimentary rocks, as well as can offer a theoretical foundation for lacustrine shale oil exploration and development.

1. Introduction

Shale is a sedimentary rock with fine-grained texture and fissility, as well as a broader class of mudstone (Aplin and Macquaker, 2011). Shale having TOC > 2 % refers to organic-rich shale (Hosterman and Whitlow, 1980), which turns out to be a vital source of hydrocarbons, shale oil, and gas reservoir, and seal rock in conventional reservoirs (Abouelresh and Slatt, 2012; Liang et al., 2018). Organic-rich shale has generated oil resources, which have been stored in the organic-rich intervals or transported into adjacent, continuous organic-poor intervals (Jarvie,

* Correspondence to: D. Khan, State Key Laboratory of Ore Deposit Geochemistry, Institute of Geochemistry, Chinese Academy of Sciences, Guiyang 550081, China.
** Corresponding author.
E-mail addresses: danish20124@yahoo.com (D. Khan), qiulwsd@163.com (L. Qiu).

https://doi.org/10.1016/j.chemer.2023.125978
Received 13 April 2022; Received in revised form 21 February 2023; Accepted 13 March 2023
Available online 16 March 2023

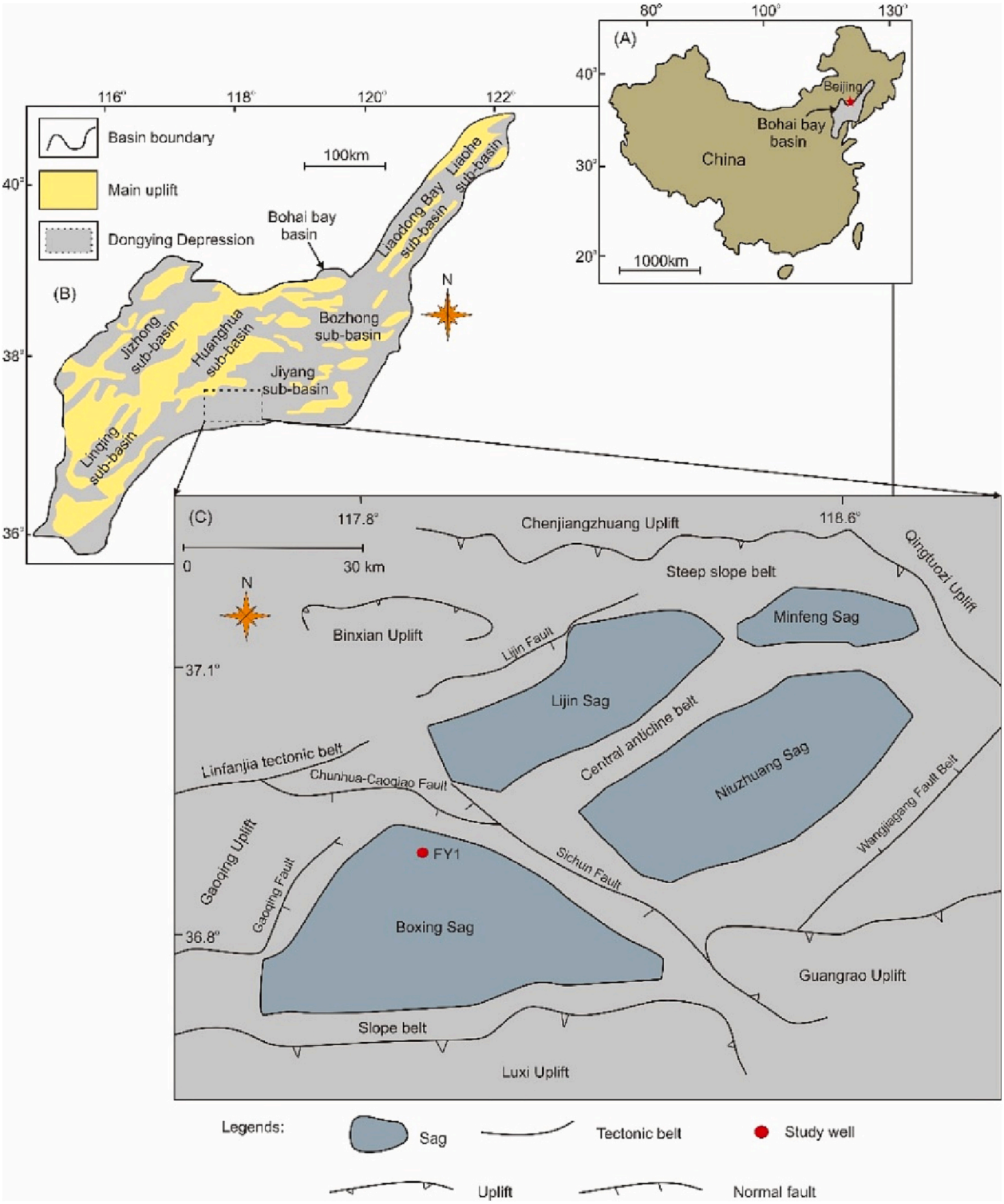

Fig. 1. Regional geological background and location map of the study wells (after Liang et al., 2018). (A) Geographic map of China showing the location of the Bohai Bay Basin, (B) a Geological map of the Bohai Bay Basin showing the location of the Dongying Depression, (C) a Geologic map showing the location of the Boxing Sag in the Dongying Depression and the study well.

2012). Organic-rich lacustrine shales account for nearly 20 % of conventional oil resources, but also turn out to be even more important in unconventional oil and gas reservoirs worldwide (e.g., Bohacs et al., 2000; Katz and Lin, 2014; Xie et al., 2016). Shale oil investigation often employs a variety of tools and experiments to access the quality of the shale petroleum system. For example, high gamma-ray values, high resistivity values, and low rock densities are the favorable petrophysical properties to indicate marine shales, but these petrophysical indicators are not always suitable for the assessment of lacustrine shale due to substantial heterogeneities in the geochemistry, lake water salinity, and depositional environment (Martel, 2013). Lacustrine shales enriched with organic matter are extensively deposited and distributed all over China, for example, in the Eocene Shahejie Formation in the Bohai Bay Basin of eastern China (Liang et al., 2017, 2018; Khan et al., 2021), the

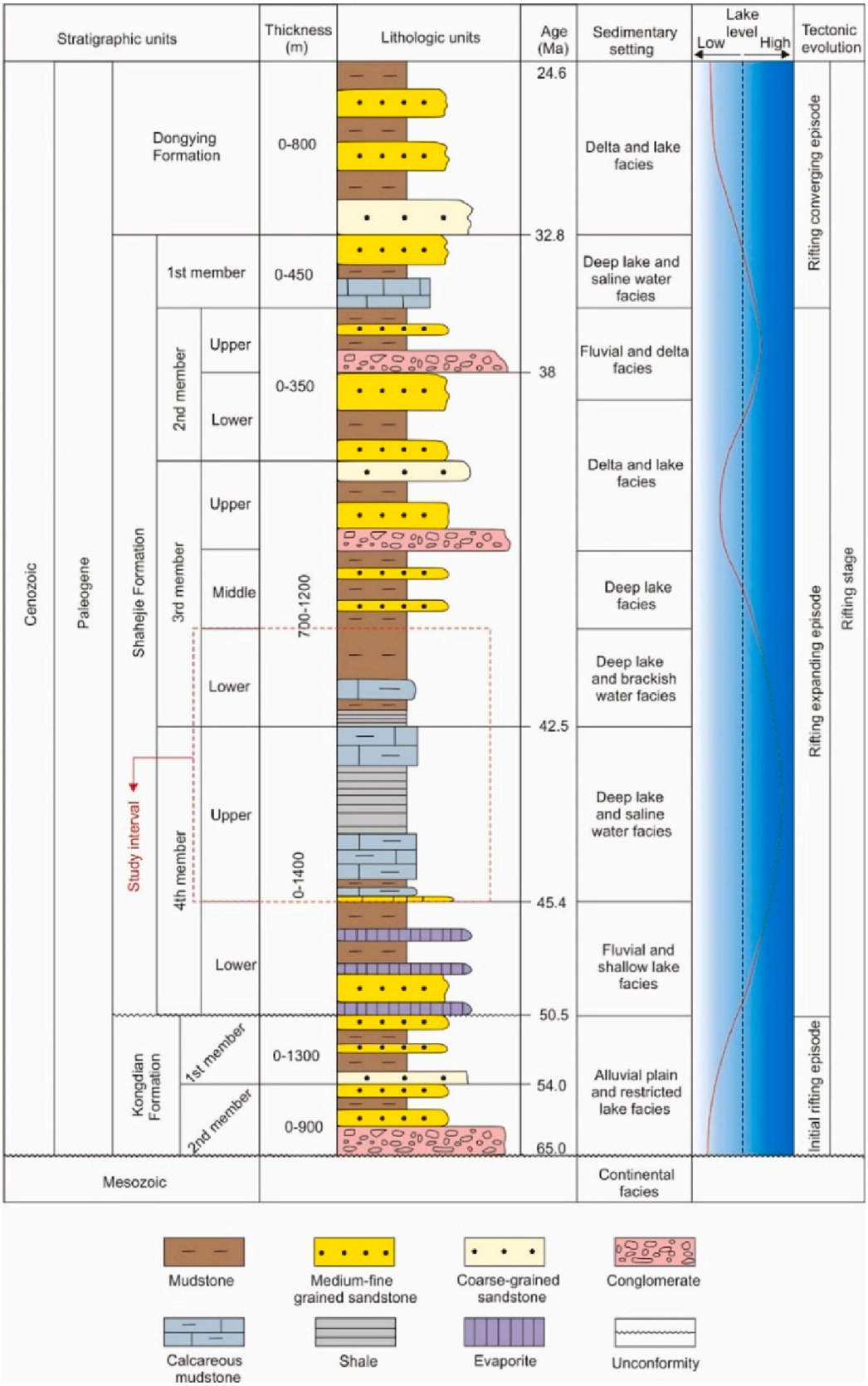

Fig. 2. The stratigraphic column of the Paleogene in Boxing Sag, Dongying Depression, Bohai Bay Basin (after Khan et al., 2021). The strata in the red box show the interval of investigation. (For interpretation of the references to color in this figure legend, the reader is referred to the web version of this article.)

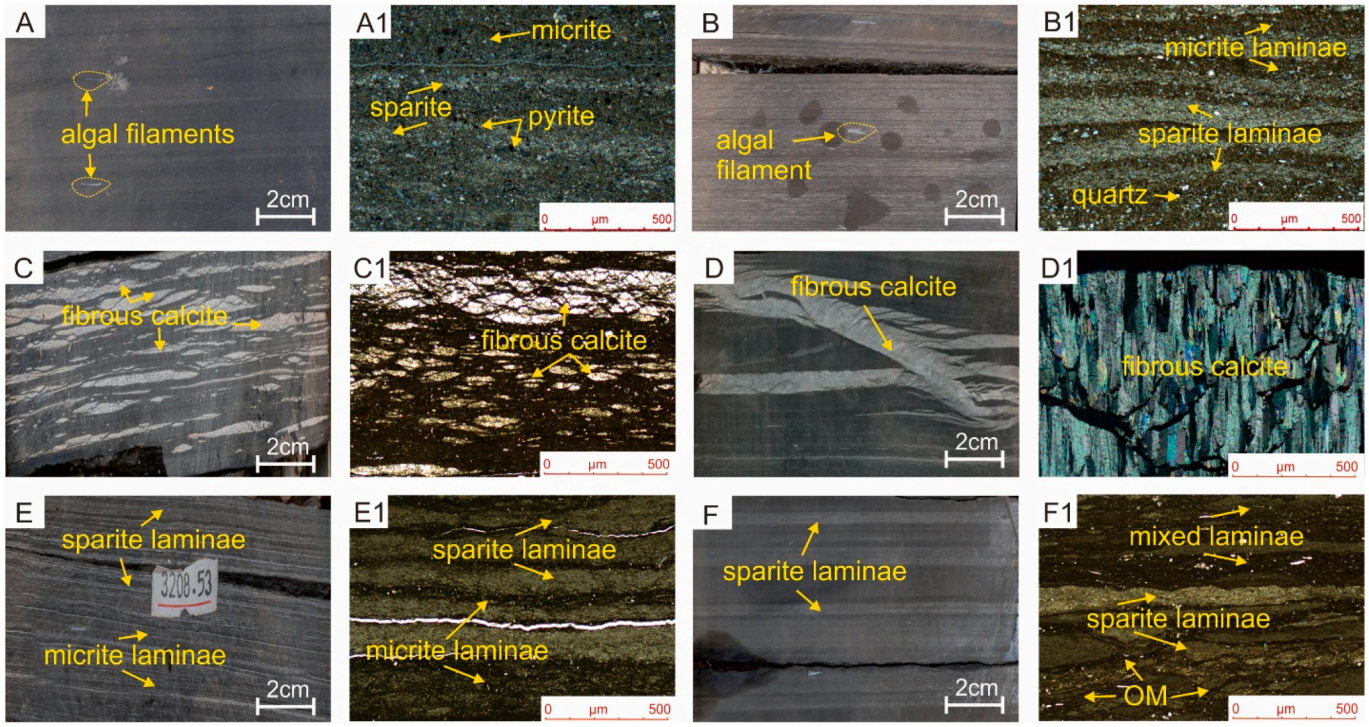

Fig. 3. Core and thin section photomicrographs showing the different fabrics of the Es_3^L-Es_4^U shale in the study area. (A-A1) 3160.40 m, FY1 well. (B—B1) 3166.40 m, FY1 well. (C—C1) 3180.60 m, FY1 well. (D—D1) 3207.83 m, FY1 well. (*E*-E1) 3208.53 m, FY1 well. (F—F1) 3295.58 m, FY1 well.

Upper Cretaceous Qingshankou Formation, and Nenjiang Formation in Songliao Basin in the northeastern part of China (Bechtel et al., 2012), the Upper Jurassic Yanchang Formation in Ordos Basin in central China (Zhang et al., 2020), and the Middle Permian Lucaogou Formation in Junggar Basin and Santanghu Basin in northwestern China (Liu et al., 2017). Lacustrine shales have restricted geographical distributions, high stratigraphic variability, mixed kerogen types, and enormous TOC variations when compared to their marine counterparts. This necessitates rigorous characterization of lacustrine mudstones to better understand the characteristics of the depositional environment and guide hydrocarbon exploration and production of shale oil.

Depositional parameters influence stratigraphic heterogeneity in lacustrine strata because lacustrine basins are particularly vulnerable to climatic variations and local tectonic effects (Bohacs et al., 2000; Carroll and Bohacs, 2001; Gonçalves, 2002; Jia et al., 2013; Katz and Lin, 2014; Khan et al., 2022b). Previous literature on lake basins has suggested that the depositional parameters represent a balance between water and sediment supply, as well as potential accommodation (Bohacs et al., 2000; Carroll and Bohacs, 2001). Rapid changes in lake water salinity, pH, lake level, and biota are caused by climatic changes, while tectonic subsidence modifies basin form and potential accommodation, and tectonics also controls the sedimentation rate in the lake (Carroll and Bohacs, 2001; Ma et al., 2017: Liang et al., 2017, 2018). These above parameters are mostly dependent on macroscopic lithofacies changes, and their applicability to lacustrine shales with minor stratigraphic diversity at the smaller scale has yet to be determined. Current research on marine mudstone have shown that combining sedimentological examinations of core samples at both macroscopic and microscopic scales with whole-rock geochemical observations are effective measures to characterize shale heterogeneity and provide insight into depositional parameters, organic matter (OM) accumulation and preservation, and chemistry of paleowater (Loucks and Ruppel, 2007; Hammes and Frébourg, 2012; Könitzer et al., 2014; Bruner et al., 2015; Ma et al., 2019; Green et al., 2020; Cichon-Pupienis et al., 2021). The use of such integrated research on lacustrine mudstone is uncommon, yet it is effective in detecting stratigraphic variability.

In the Dongying Depression (DD), shale lithofacies and depositional environment were previously examined, logged, and characterized in outcrops and drilling cores, using a simple descriptive methodology that only permitted the differentiation between argillaceous limestones and calcareous mudstones (Li et al., 2015). In this research work, we used TOC contents, mineral contents, elemental geochemistry, and sedimentary structures to characterize shale lithofacies and elucidate the depositional environment. This study describes the results of a comprehensive investigation of TOC content, mineralogical composition, elemental geochemistry (major, minor, and trace elements), and sedimentary structures found within Es_3^L-Es_4^U shale of the Eocene Shahejie Formation in the Boxing Sag, Dongying Depression. From this analysis, we propose a simple classification of shale lithofacies is proposed which is based on the above four parameters. The depositional environment of the Es_3^L-Es_4^U shale of the Eocene Shahejie Formation was also studied based on elemental geochemistry and mineralogy analyses including paleoclimate, paleosalinity, provenance, paleoredox, detrital influx, and water depth. The prime objectives of this study are, (1) to explain the mineralogical and geochemical attributes of the lacustrine shale, (2) and their control on the depositional environment in the Eocene Dongying Depression, Bohai Bay Basin. This study can be useful to provide a simple approach to characterizing shale lithofacies scheme for lacustrine sediments and the insights of various parameters to interpret the depositional environment. The interpretations deduced from the current research work are likely to expand the knowledge of shale lithofacies and the genesis of lacustrine fine-grained sedimentary rocks, as well as can offer a theoretical foundation for lacustrine shale oil exploration and development.

2. Geological setting

The Bohai Bay Basin (BBB) is a Cenozoic rift basin located on the eastern coast of China, with an areal extent of approximately 200,000 km^2 (Fig. 1). BBB is divided into seven sub-basins namely, the Linqing, Jizhong, Jiyang, Changwei, Huanghua, Bozhong, and Liaohe, sub-basins, from northeast to southwest (Fig. 1) (Hao et al., 2011; Huang

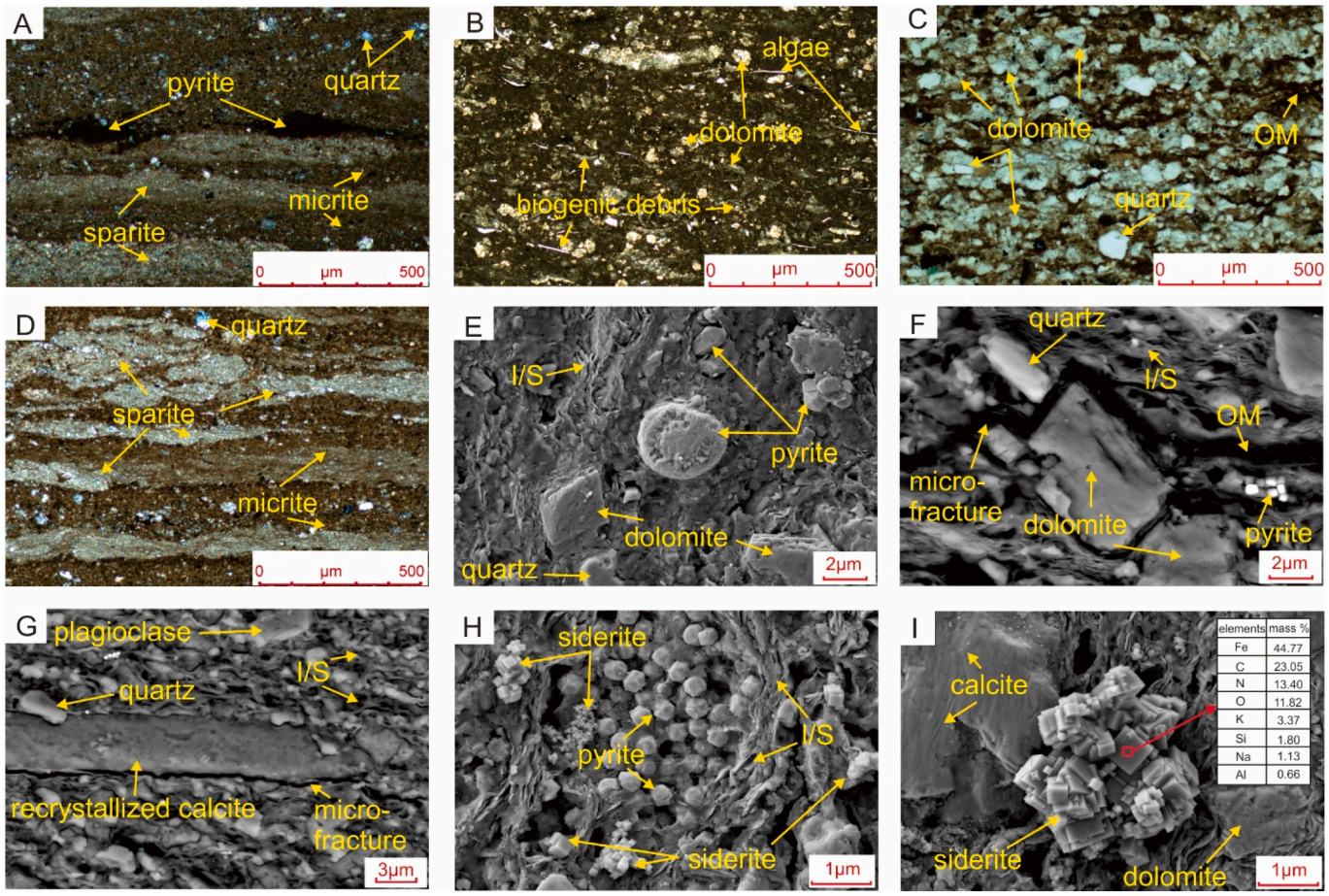

Fig. 4. Photomicrographs of the thin sections and FE-SEM showing the characteristics and distribution of different minerals in the study area. (A) 3184.10 m, FY1 well. (B) 3311.81 m, FY1 well. (C) 3170.35 m, FY1 well. (D) 3146.80 m, FY1 well. (E) 3207.80 m, FY1 well. (F) 3239.85 m, FY1 well. (G) 3239.85 m, FY1 well. (H) 3390.94 m, FY1 well. (I) 3390.94 m, FY1 well.

et al., 2012). Among these sub-basins, the Jiyang sub-basin is a rift basin of the Mesozoic to Cenozoic age in the southeast of BBB (Zhu et al., 2013). It is composed of four secondary depressions: Dongying, Huimen, Zhanhua, and Chezhen, which are separated by Chengdong Uplift, Chenjiazhuang Uplift, and Yihezhuang Uplift (Fig. 1). The Dongying Depression is located in the southeast of the Bohai Bay Basin, in eastern China. It covers an area of 5700 km^2 and is bounded by the Luxi and Guangrao uplifts in the south, the Chenjiazhuang uplift, and Binxian uplift in the north, the Qingtuozi uplift in the east, and the Linfanjia tectonic belt and Gaoqing uplift in the west (Liang et al., 2017). The Dongying Depression comprises several secondary morpho-tectonic sectors including the Boxing Sag, Lijin Sag, Niuzhuang Sag, Minfeng Sag, northern steep slope belt, central anticline belt, and southern slope belt (Jiang et al., 2011). Boxing Sag is located in the southwestern part of the Dongying Depression in the Bohai Bay Basin, eastern China. It covers an area of 1320 km^2 approximately and is bounded by the Sichun Fault in the east, the Gaoqing Fault in the west, the Luxi Uplift in the south, and the Chunhua-Caoqiao Fault in the north (Yuan and Jiang, 2000; Si and Zhang, 2008).

Stratigraphically, it is composed of Cenozoic strata including the Kongdian, Shahejie, and Dongying formations (Fig. 2). The Eocene Shahejie Formation is further divided into four members i.e. 1st member, 2nd member (upper and lower), 3rd member (upper, middle, and lower), and 4th member (upper and lower) (Fig. 2). The lower 3rd member (Es_3^L) and upper 4th member (Es_4^U) are deposited in a lacustrine environment and are interpreted as the stratigraphic record of the main rifting expansion episode in which the relative lake level reached a maximum (Xue et al., 2013; Liang et al., 2017). The high level of organic productivity coupled with anoxic conditions and rift basin subsidence resulted in the deposition of organic-rich black shale (approximately 400 m) in the Es_3^L-Es_4^U shale in the Dongying Depression. The organic-rich shale from these two shale members is the interval of interest of this research work.

3. Material and methods

3.1. Sample collection

The shale samples were collected from the Es_3^L-Es_4^U shale of the Eocene Shahejie Formation in the Boxing Sag, Dongying Depression. The representative core samples were obtained for this research work from FY1 well in the study area. The study interval of the Es_3^L and Es_4^U shale members ranges from 2937.8 m to 3140.25 m (Fig. 2). The lithology of the Es_3^L-Es_4^U shale is comprised of grayish to dark-gray fine-grained lacustrine calcareous shale.

3.2. Sample preparation and thin-section analysis

Thin sections are made from the research interval's core samples. Core samples were crushed and grounded to attain a standard thickness of 0.03 mm. After a thorough examination of hand specimens that reflect the main features of the $Es3^L$-$Es4^U$ shale, 140 thin sections were prepared for petrographic analysis, by using a polarizing microscope (Model: Leica DM4).

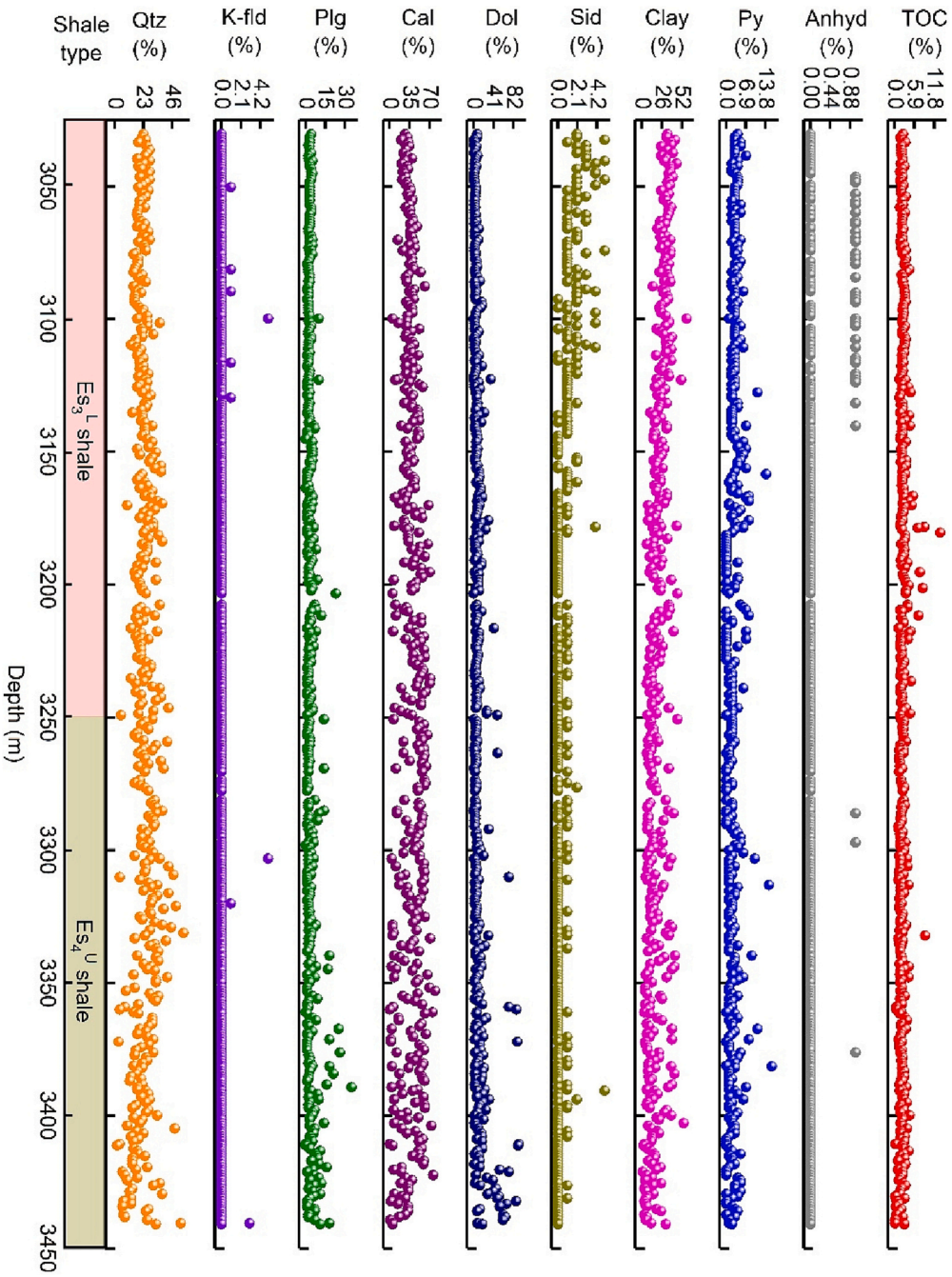

Fig. 5. The compositional characteristics and distribution of different mineral types of the Es_3^L-Es_4^U shale from the FY1 well in the Boxing Sag. Note: Qtz = quartz, K-feld = K-feldspar, Plg = plagioclase, Cal = calcite, Dol = dolomite, Sid = siderite, Py = pyrite, Anhyd = anhydrite, TOC = total organic carbon.content.

3.3. XRD analysis

A total of 403 samples from the Es_3^L-Es_4^U shale were chosen and analyzed for whole-rock mineralogical composition by Panalytical X'Pert PRO X-ray diffractometer enabled with a Cu X-Ray target (40 kV, 40 mA). Each sample weighing 5 g was oven-dried at 40 °C for two days and grounded to <40 mm size to disperse the mineral fractions by agate mortar. The angle range for the analysis was 5° - 10°. Identification of various phases of different minerals and their relative abundances (wt%) were calculated by using computer diffractogram analysis.

3.4. TOC and Rock-Eval analyses

The TOC content is a key factor for the source rocks evaluation because it reflects the distribution of organic matter (OM). A total of 403 representative shale samples were chosen for TOC (total organic carbon) using a carbon and sulfur analyzer (Model: LECO CS744) that worked at 1200 °C in a closed system. The shale samples <100 mesh in size, then 0.13 g–0.14 g of each sample was added in a container. These samples were soaked in a diluted HCl solution (volume ratio = 1:7) for 24 h to remove inorganic carbonate contents. The samples were washed with distilled water to eliminate acid impurities and placed in an oven for two hours at 60 °C. Each sample was placed in the LECO CS744 analyzer for TOC analysis.

Rock-Eval pyrolysis is a very well-known screening method used for the bulk characterization of OM in sediments and it provides information regarding hydrocarbon contents, kerogen types, maturity, and hydrocarbon generation potential (Scheeder et al., 2020). The maximum

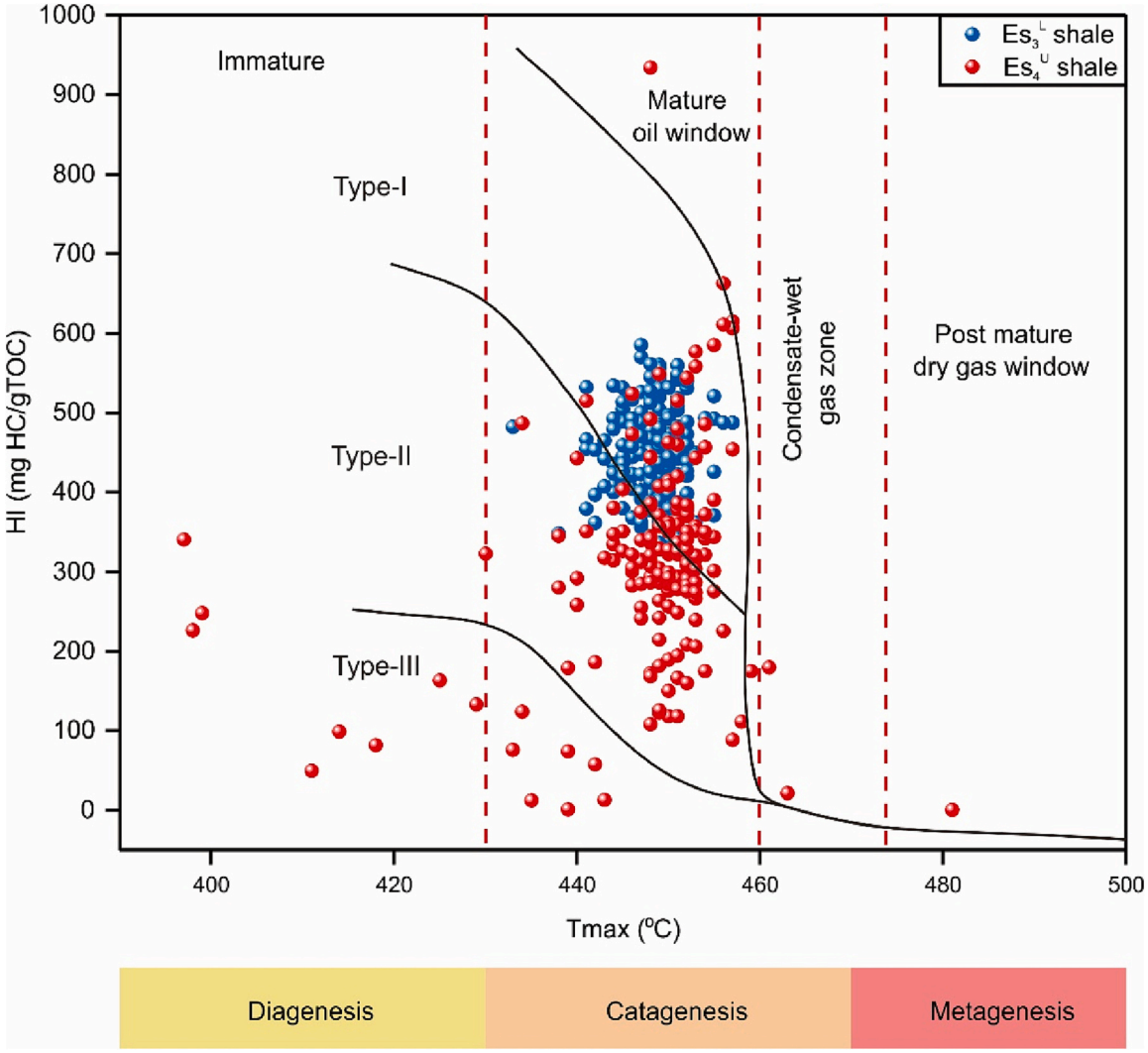

Fig. 6. Determination of kerogen type with Rock-Eval analysis in the study area (Boxing Sag). Scatterplot of hydrogen index (HI) vs Tmax temperature for Es_3^L–Es_4^U shale, showing the kerogen types (type-I kerogen, type-II kerogen, and type-III kerogen) and thermal maturity stages. A genetic pathway for individual kerogen types after Scheeder et al. (2020).

pyrolysis temperature (Tmax) corresponds to the temperature with the highest S2 peak; free hydrocarbon (S1) is the hydrocarbon content at 300 °C; hydrocarbon (S2) is generated and measured when the samples were heated from 300 °C to 600 °C at a rate of 25 °C/min; the maximum pyrolysis temperature (S1) is the hydrocarbon content at 300 °C. Other parameters such as the hydrogen index (HI), production index (PI), and vitrinite reflectance (R_o) were also calculated. A total of 24 shale samples were selected for Rock-Eval analysis during this research work.

3.5. XRF and field emission scanning electron microscopy (FE-SEM) analyses

A total of 208 shale samples were carefully chosen for inorganic geochemical analysis. The distribution and abundance of different elements (major, minor, and trace elements) were calculated by 'M4 Tornado (Bruker)' micro X-ray fluorescence (XRF) spectrometer, with a voltage of 50 kV, and a current of 600 μA. A 25 μm beam size, using a time of 5 μs/pixel was used in this analysis.

Based on thin-section observation and mineral composition, a total of 10 representative shale samples with different mineralogy and textures were cautiously selected for field-emission scanning electron microscopy (FE-SEM) analysis to observe the arrangement and distribution of different minerals, OM, various pores, and microfractures. The representative samples were polished with argon ions and then coated with platinum to enhance the conductivity. The analysis was completed on a Zeiss Crossbeam-550 (Gemini-2) SEM coupled with an energy dispersive spectrometer (EDS) system which is used to analyze the elemental composition of different minerals.

4. Results

4.1. Sedimentary fabrics

The sample set shows considerable variability in bedding and lamination at the macroscopic and microscopic scale (Fig. 3). The majority of shale samples have distinct parallel laminations that correspond to texture, mineral composition, and organic matter variations. A few samples have homogenous sedimentary fabrics. In all of the samples, the larger particles are mainly skeletal grains, predominantly algal filaments, and other small biogenic fragments. Laminated samples do not show evidence of bioturbation (Fig. 3).

4.2. Mineralogical composition

Carbonate, clay minerals, quartz, plagioclase, K-feldspar, pyrite, and anhydrite make up the Es_3^L-Es_4^U shale in the study area (Fig. 4–5,

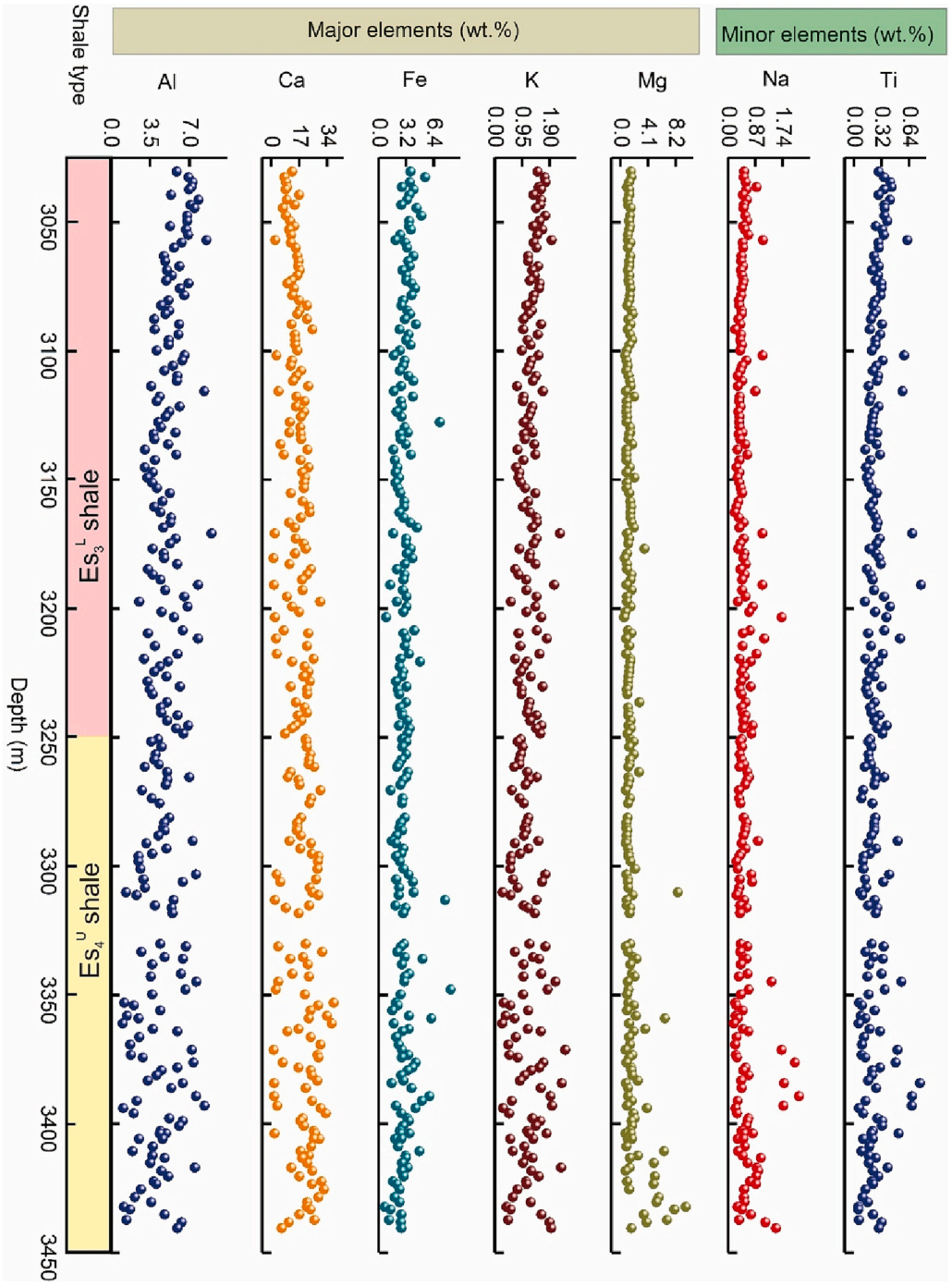

Fig. 7. The distribution of major and minor elements in the Es_3^L-Es_4^U shale of the Boxing Sag.

Table S1). Carbonates are the most common minerals with an average of 51.47 %. Of these carbonates, calcite is ranging from 0 %–80 %. The amount of calcite is inversely proportional to dolomite content in the study area (Fig. 5). Calcite is mostly found in clay- to silt-sized crystalline form in the Es_3^L-Es_4^U shale, and it contains a small quantity of calcareous biological fragments, such as ostracods. Dolomite is ranging from 0 %–93 % (Fig. 5). Dolomite is generally found in clay-sized crystalline form, as dolomite laminae or isolated dolomite crystals. The siderite ranges from 0 % to 5 % with an average of 0.86 % and its content decreases with increasing burial depth (Fig. 5). The content of quartz, K-feldspar, and plagioclase are 2 % to 55 % (avg. 23.8 %), 0 % to 5 % (avg. 0.05 %), and 0 % to 35 % (avg. 3.9 %), respectively (Fig. 5). The content of quartz decreases with increasing burial depth while the content of plagioclase increases with increasing burial depth (Fig. 5). The clay and pyrite contents are 1 % to 58 % (avg. 20.8 %) and 0 % to 16 % (avg. 2.8 %), respectively. The clay and pyrite contents increase with increasing depth (Fig. 5). The content of anhydrite is found negligible (avg. 0.1 %) in this shale (Fig. 5). The outcomes also demonstrate the apparent variability of mineral concentration across stratigraphic sub-members.

4.3. *Organic geochemistry*

The bulk organic geochemical data indicate that TOC content is ranging from 0.08 wt% to 13.6 wt% (avg. 2.45 wt%) in the studied shale samples (Fig. 5). The concentration of free hydrocarbon (S1) varies from

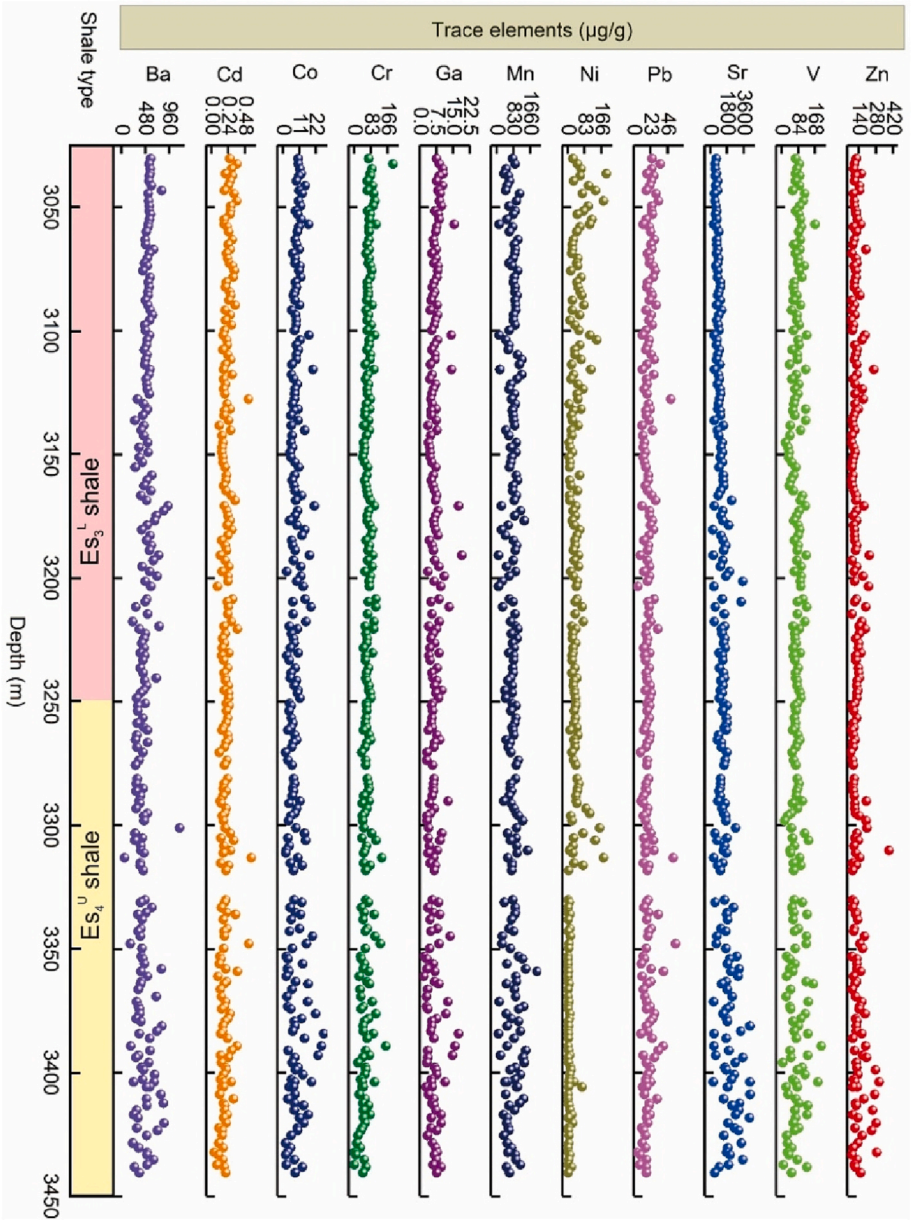

Fig. 8. The distribution of trace elements in the Es_3^L-Es_4^U shale of the Boxing Sag.

1.02 mg/g to 5.36 mg/g (avg.2.76 mg/g) in the Es_3^L-Es_4^U shale (Table S2). The concentration of thermally cracked hydrocarbon (S2) ranges from 2.53 mg/g to 41.22 mg/g (avg. 10.41 mg/g) (Table S2). The maximum temperature (Tmax) values are between 425 °C to 454 °C (avg. 446.78 °C) (Table S2). Additionally, Rock-Eval analysis reveals that the values of HI (hydrogen index) mainly range from 1 mg/g TOC to 16.4 mg/g TOC (avg. 4.14 mg/g TOC) (Table S2). The comparison plot between pyrolysis-based Tmax and HI was used to categorize the OM, revealing the predominance of type I and type II kerogens, however, type III kerogens were also found in a few samples (Fig. 6). The predominance of type I and type II kerogens is explained by the fact that the organic matter is mostly derived from planktonic algae such as Bohai algae, ditch whip algae, and coccoliths (Wang, 2012; Liang et al., 2017). The thermal maturity of the source rock can be predicted by using the Tmax pyrolysis parameters (Peters, 1986). The Tmax values of the studied samples indicate that the OM is mature and reaches the mature oil window (Fig. 6). The high PI values (avg. 0.23) also demonstrate high maturity and higher oil generation potential. Furthermore, the vitrinite reflectance (R_o) of the studied shale is calculated by using the Jarvie et al. (2007) formula. R_o values range from 0.49 % to 1.01 % with an average of 0.88 % (Table S2), which further confirms the maturity of the studied shale in the Boxing Sag, Dongying Depression. The red dots on the left side show immature samples of the Es_4^U shale in the study area (Fig. 6).

4.4. Inorganic geochemistry

The bulk assemblage of major, minor, and trace elements is shown in Fig. 7–8 (Table S3). The XRF results indicate that the concentration of major elements (elements >1 %) are Al (ranges from 1.08 % to 8.94 %, avg. 4.7 %), Ca (ranges from 1.37 % to 37.7 %, avg. 17.3 %), Fe (ranges from 0.67 % to 8.34 %, avg. 2.9 %), K (ranges from 0.25 % to 2.43 %, avg. 1.2 %), and Mg (ranges from 0.51 % to 9.68 %, avg. 1.6 %) in the studied shale (Fig. 8). Minor elements (elements range from 1 to 0.1 %) include Na (avg. 0.54 %) and Ti (avg. 0.25 %) (Fig. 8), and trace elements (<100 ppm) are Ba (avg. 478 μg/g), Cd (avg.0.21 μg/g), Co (avg. 8.77 μg/g), Cr (avg. 64.59 μg/g), Ga (avg. 6.79 μg/g), Mn (avg. 779.6 μg/g), Ni (avg. 34.28 μg/g), Pb (avg. 20.11 μg/g), Sr (avg. 1388.9 μg/g),

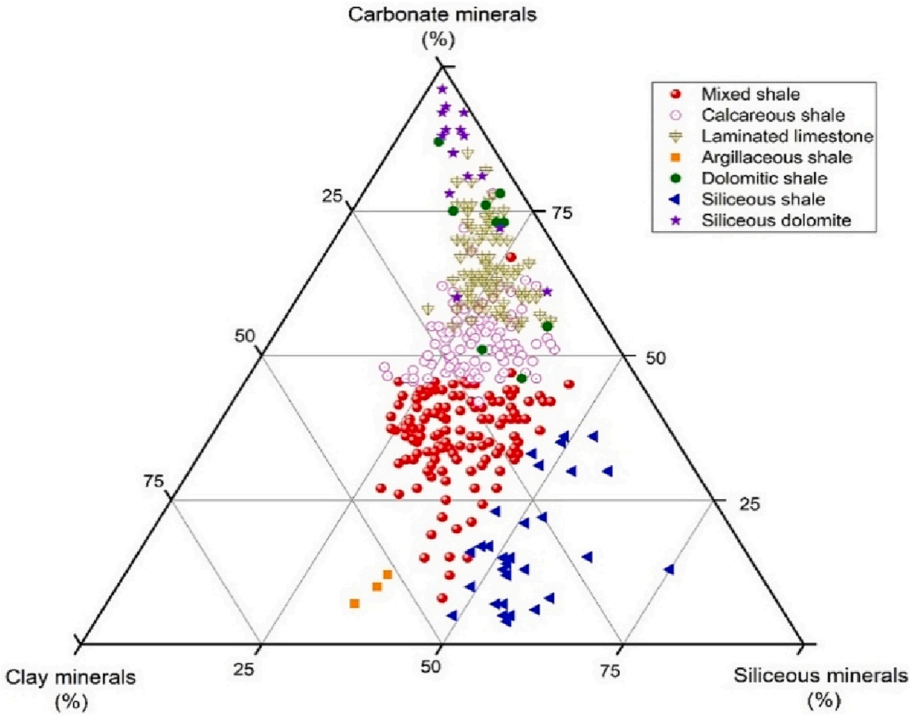

Fig. 9. Ternary diagram showing the distribution of different lithofacies of the Es_3^L–Es_4^U shale in the Boxing Sag, Dongying Depression.

Table 1
Showing the distribution of minerals in various lithofacies of the Es_3^L–Es_4^U shale. Note: A–B (C) where A = minimum value, B = maximum values, C = average value, MSL = Mixed shale lithofacies, CSL = Calcareous shale lithofacies, LLL = Laminated shale lithofacies, ASL = Argillaceous shale lithofacies, DSL = Dolomitic shale lithofacies, SSL = Siliceous shale lithofacies, SDL = Siliceous dolomite lithofacies.

Lithofacies	Siliceous minerals (%)	Carbonate minerals (%)	Clay minerals (%)	TOC (%)
MSL	21–46 (33.92)	8–67 (36.20)	7–46 (29.60)	1.29–9.05 (2.60)
CSL	17–40 (28.50)	42–78 (52.88)	4–34 (18.69)	1.26–8.35 (2.53)
LLL	11–37 (23.91)	55–85 (65.26)	3–23 (10.95)	1.01–13.6 (2.40)
ASL	34–36 (35.2)	7–12 (9.6)	51–58 (54.4)	1.76–3.25 (2.48)
DSL	6–38 (22.63)	46–87 (67.90)	3–19 (9.36)	1.18–2.97 (2.01)
SSL	46–75 (53.68)	4–36 (17.31)	11–46 (29.53)	0.08–7.08 (3)
SDL	2–34 (12.29)	60–96 (82.41)	1–18 (5.94)	0.11–2.42 (1.07)

V (76.53 μg/g), and Zn (127.14 μg/g) in the $Es3^L$ and $Es4^U$ shale of the study area (Fig. 8, Table S3). The amount of major and minor elements varies with increasing burial depth in the study area (Fig. 7). While the quantity of the majority of the trace elements is relatively uniform from top to bottom of the studied samples in the Boxing Sag, Dongying Depression (Fig. 8).

In this study, a variety of different elements are used as a proxy to predict the parameters of the depositional environment, for example, C.I (Climate index) and C.I.A (Chemical index of alteration) proxies were used to interpret the climatic conditions (Nesbitt and Young, 1982; Bahlburg, 2009; Moradi et al., 2016; Ding et al., 2018; Li et al., 2019; Awan et al., 2020). The C.I. values range from 0.1 to 2.27 (avg. 0.60), while the values of C.I.A ranges from 0.61 to 0.79 (avg. 0.73) in the studied shale samples. The ratios of Sr/Ba (ranges from 0.41 to 17.80 with an average of 3.14) and Ca/Ca + Fe (ranges from 0.22 to 0.96 with an average of 0.81) were taken as proxies to estimate the paleosalinity (Liu, 1980; Deng and Qian, 1993; Hu et al., 2012). Ti/Al and Al/Al + Fe ratios were used to estimate the detrital influx (Boström et al., 1973; Murphy et al., 2000; Liu et al., 2015; Niu et al., 2018). The values of Ti/Al vary from 0.024 to 0.11 (avg. 0.051), whereas the values of Al/Al + Fe range from 0.20 to 0.86 with an average of 0.60 in the Es_3^L and Es_4^U shale in the study area. Al/Ti (vary from 8.38 to 41.60 with an average of 20.19) and *V*/V + Ni (ranges from 0.23 to 0.99 with an average of 0.74) values were used to estimate the provenance of sediments and paleoredox conditions of the lake environment, respectively (Lewan, 1984; Mongenot et al., 1996; Moradi et al., 2016). The ratios of Fe/Ca + Mg are used to analyze lacustrine water depth (Restituito, 1987; Chen et al., 2016). The values of Fe/Ca + Mg range from 0.021 to 2.45 with an average of 0.25 in the Es_3^L and Es_4^U shale of the Boxing Sag, Dongying Depression.

4.5. *Lithofacies description*

Shale lithofacies has been established based on sedimentary characteristics, mineralogy, and TOC content. In this study, seven lithofacies have been established including mixed shale, calcareous shale, laminated limestone, argillaceous shale, dolomitic shale, siliceous shale, and siliceous dolomite (Fig. 9). Shale is further divided into laminated shale and non-laminated shale based on sedimentary structures, while organic-rich shale (>2 % TOC) and organic-poor shale (<2 % TOC) are based on TOC contents.

4.5.1. *Mixed shale*

Mixed shale lithofacies (MSL) is characterized by low clay mineral contents (avg. 29.6 %), moderate carbonate minerals (avg. 36.2 %), and siliceous minerals (avg. 33.9 %) (Table 1). This lithofacies is rich in OM, and the TOC content is ranging from 1.29 to 9.05 % with an average of 2.60 % (Table 1). Some intervals have well-developed laminations while others have no laminations (Fig. 10A–B). Few algal fragments can also be seen in the non-laminated intervals of this shale (Fig. 10A). Micrite, sparite, and clay laminae are frequently observed in the laminated

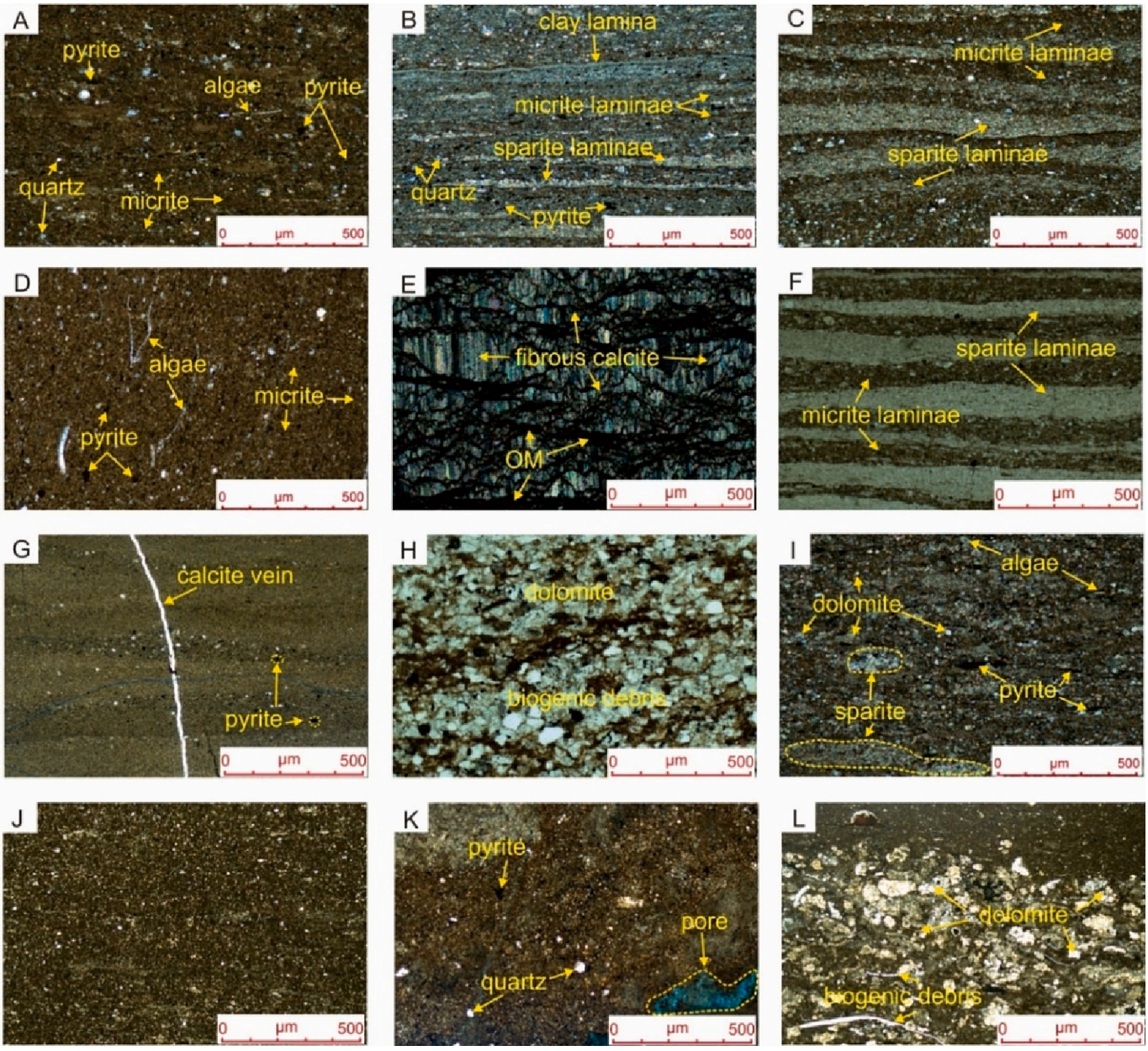

Fig. 10. Photomicrographs of the thin sections show the characteristics of different lithofacies in the study area. (A) mixed shale, well FY1, 3107 m, plane-polarized light (PPL). (B) mixed shale, well FY1, 3152.80 m, PPL. (C) calcareous shale, well FY1, 3166.40 m, PPL. (D) calcareous shale, well FY1, 3249.10 m, PPL. (E) laminated limestone, well FY1, 3199.40 m, PPL. (F) laminated limestone, well FY1, 3272.30 m, PPL. (G) argillaceous shale, well FY1, 3371.68 m, PPL. (H) dolomitic shale, well FY1, 3170.35 m, PPL. (I) dolomitic shale, well FY1, 3246.40 m, PPL. (J) siliceous shale, well FY1, 3215.88 m, PPL. (K) siliceous shale, well FY1, 3237 m, PPL. (L) siliceous dolomite, well FY1, 3311.81, PPL.

intervals of mixed shale lithofacies (Fig. 10B). In the Es_3^L-Es_4^U shale, mixed shale has a greater growth frequency. It is mainly developed in the upper part of the Es_3^L-Es_4^U shale.

4.5.2. Calcareous shale

This lithofacies is represented by higher carbonate minerals (52.8 %), low siliceous (28.5 %), and clay minerals (18.6 %) (Table 1). Calcareous shale lithofacies (CSL) are also categorized as organic-rich shale because TOC content in this lithofacies ranges from 1.26 to 8.35 % with an average of 2.53 % (Table 1). Primary sedimentary structures (laminations) are also observed in some sections while some sections lack laminations (10C—D). In laminated shale, light-colored laminae show sparite while brown-colored laminae show micrite (Fig. 10C). Micrite and sparite laminae are detected in the laminated intervals of calcareous shale lithofacies (Fig. 10C). Few algal fragments can also be observed in the non-laminated intervals of this shale (Fig. 10D). Calcareous shale is the most dominant lithofacies after mixed shale in the Es_3^L-Es_4^U shale.

4.5.3. Laminated limestone

This lithofacies is composed of higher carbonate minerals (avg. 55–85 %) especially calcite minerals which range from 51 to 80 % with an average of 58.5 % with subordinate dolomite (avg. 6.4 %) and siderite (0.3 %) (Table 1). The concentration of siliceous minerals (avg. 23.9 %) and clay minerals (10.9 %) is very low in this lithofacies. TOC content is ranging from 1.01 to 13.6 % (avg. 2.40 %) (Table 1). Lamination is frequently observed in this lithofacies (Fig. 10E–F). Recrystallization of micrite to sparry calcite is also common in this facies

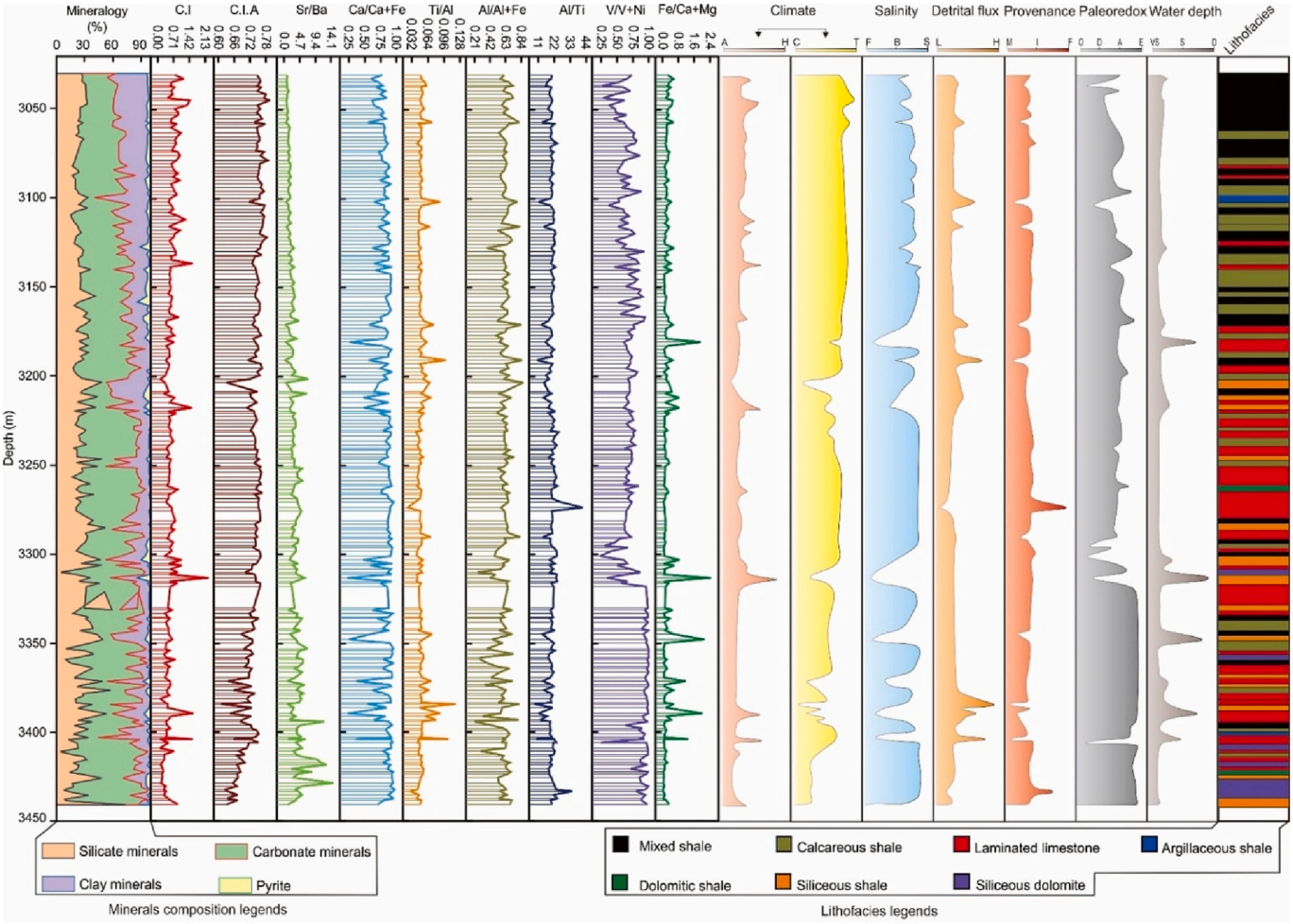

Fig. 11. The characteristics of the sedimentary environment of the $Es3^{L}$–$Es4^{U}$ shale, are evidenced by mineral composition and inorganic geochemical proxies. The effect of the different sedimentary environment parameters on the evolution of shale lithofacies is also shown in the figure. Note: A = arid, H = humid, C = cold, T = temperate, F = fresh, B = brackish, S = saline, L = low, H = high, M = mafic, I = intermediate, F = felsic, O = oxic, D = dysoxic, A = anoxic, E = Euxinic, VS = very shallow, S = shallow, D = deep.

Table 2
Lithofacies distribution and the sedimentary environment characteristics in the $Es3^{L}$–$Es4^{U}$ shale of the Shahejie Formation in FY1 well of the Boxing Sag, Dongying Depression.

Lithofacies	Climate	Salinity	Terrestrial input	Provenance	Redox conditions	Water depth
Mixed shale	Semi-humid	Brackish-saline	Restricted input	Intermediate	Anoxic	Moderate
Calcareous shale	Semi-humid	Saline	Restricted input	Intermediate	Anoxic	Moderate
Laminated limestone	Semi-arid	Saline	Restricted input	Intermediate	Anoxic	Moderate
Argillaceous shale	Semi-arid	Saline	Moderate input	Intermediate	Anoxic	Moderate
Dolomitic shale	Semi-arid	Saline	Restricted input	Intermediate	Anoxic	Moderate
Siliceous shale	Humid	Brackish-saline	Moderate input	Intermediate	Anoxic	Deep
Siliceous dolomite	Semi-arid	Saline	Restricted input	Felsic	Euxinic	Shallow

(Fig. 10E). During recrystallization, various microfractures are developed which are filled with OM. Fibrous calcite is also observed in the laminated limestone lithofacies (LLL) (Fig. 10E). Light-colored laminae show sparry calcite while brown-colored laminae represent micrite (Fig. 10F).

4.5.4. Argillaceous shale

This shale is characterized by a higher amount of clay minerals (avg. 54.4 %) than carbonate minerals (avg. 9.6 %) and siliceous minerals (avg. 35.2 %) (Table 1). In this lithofacies, clay minerals are ranging from 51 to 58 %. Among siliceous minerals, quartz (avg. 20.4) is the most abundant mineral with a subordinate concentration of plagioclase (avg. 11.6 %) in this lithofacies (Table 1). Lamination is poorly developed in this shale (Fig. 10G). Argillaceous shale lithofacies (ASL) is marked by high TOC content (avg. 2.48 %) (Table 1).

4.5.5. Dolomitic shale

Dolomitic shale lithofacies (DSL) displays a high content of carbonate minerals (avg. 67.9 %), with subordinate siliceous minerals (avg. 22.6 %), and clay minerals (avg. 9.36 %) (Table 1). Among carbonate minerals, dolomite content (avg. 40 %) is higher than calcite mineral (avg. 27.3 %) (Table 1). Dolomite is present in the form of smaller crystals (Fig. 10H–I). Some algae and other biogenic debris are also observed in this lithofacies (Fig. 10H). Pyrite is developed as a

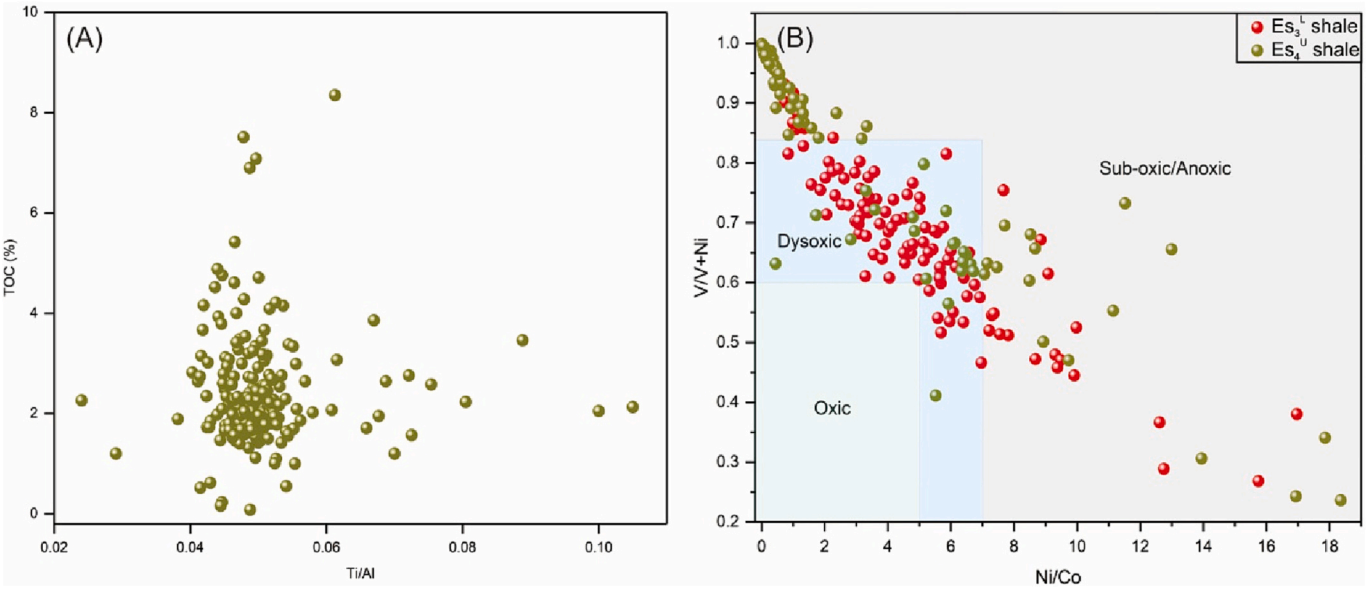

Fig. 12. (A) Scatterplot of the abnormal relationship between TOC and Ti/Al showing no effect of detrital influx dilution on OM. (B) The cross plot of Ni/Co vs V/V + Ni shows the dysoxic to anoxic conditions during the deposition of the Es_3^L–Es_4^U shale in the study area.

replacement mineral (Fig. 10I). Lenses of sparry calcite are also observed during the petrographic analysis of thin sections (Fig. 10I). TOC content is ranging from 1.18 % to 2.97 % (avg.2.01 %) (Table 1).

4.5.6. Siliceous shale

Siliceous shale lithofacies (SSL) exhibits a higher concentration of siliceous minerals (avg. 53.6 %), with subordinate clay minerals (avg. 29.5 %), and carbonate minerals (avg. 17.3 %) (Table 1). Among siliceous minerals, quartz is the most dominant mineral than K-feldspar and plagioclase in this shale (Fig. 10J–K). The content of quartz is ranging from 18 % to 55 % with an average of 37.2 %. This lithofacies has higher TOC content (avg. 3 %) (Table 1).

4.5.7. Siliceous dolomite

The concentration of dolomite is ranging from 52 % to 93 % (avg. 71.8 %) and is higher than other minerals. In siliceous dolomite lithofacies (SDL), the content of calcite is ranging from 0 to 32 % with an average of 11.8 %), while quartz and plagioclase are ranging from 2 to 26 % (avg. 9.1 %) and 0–7 % (avg. 2.29 %), respectively (Table 1). Pyrite is ranging from 0 to 4 % (avg. 1.05 %), while the average concentration of clay minerals is 5.94 % (Table 1). Crystals of dolomite are detected in the dolomite lithofacies (Fig. 10L). Some algae and other biogenic debris are also observed in SDL (Fig. 10L). The TOC content in this lithofacies is low and it is ranging from 0.11 % to 2.42 % with an average of 1.07 % (Table 1).

5. Discussions

5.1. Paleosalinity

Sr/Ba and Ca/Ca + Fe are widely used to monitor the salinity of the lake. The salinity is positively correlated with Sr/Ba ratios in both modern and ancient lacustrine environments (Wei and Algeo, 2019). A downward increasing trend of Sr/Ba is detected in the studied samples of Es_3^L–Es_4^U in the Boxing Sag. (Fig. 11). This trend suggests the evolution of brackish water (0.6 < Sr/Ba <1) to saline water (Sr/Ba >1) lake environment during the deposition of studied shale. The decrease of salinity from bottom to top may be caused by the gradual rise of the lake level due to the humid climatic conditions (Fig. 11). Additionally, Ca/Ca + Fe is also a very reliable geochemical proxy and is commonly used to reflect variations in lake water salinity through geologic time (Lan et al., 1987; Hu et al., 2012). The ratios of Ca/Ca + Fe higher than 0.8 corresponds to the saline water, ratios ranging from 0.4 to 0.8 indicates brackish water, and <0.4 indicates freshwater (Fig. 11). A downward increasing trend of Ca/Ca + Fe in the study area also suggests the transition of lake water from brackish to saline during the deposition (Fig. 11). This trend also supports the interpretations implicated by Sr/Ba ratios. Based on these interpreted ratios, the Es_3^L–Es_3^U shale was deposited in a saline environment in the study area, with an average Sr/Ba of 3.14 (>1) and Ca/Ca + Fe of 0.81 (>0.8).

MSL has an average Sr/Ba ratio of 2.44 (saline water) and a Ca/Ca + Fe ratio of 0.78 (brackish water), indicating brackish to a saline environment (Table 2). The average ratios of Sr/Ba in CSL, LLL, ASL, DSL, SSL, and SDL are 3.23, 3.85, 2.87, 3.51, 2.81, and 8, respectively (Table 2). While the average Ca/Ca + Fe ratios in CSL, LLL, ASL, DSL, SSL, and SDL are 0.84, 0.83, 0.87, 0.84, 0.65, and 0.92, respectively (Table 2). According to these interpretations, all the lithofacies except MSL and SSL are deposited in the saline water environment in the Boxing Sag, Dongying Depression.

5.2. Paleoclimatic conditions

Paleoclimate is a key parameter that affects the paleosalinity of the lake environment, and evaporation activities enhance the salinity of water in arid environmental conditions (Tao et al., 2017). Paleoclimatic conditions control the redox conditions of the water column and the influx and terrigenous material. The migration and distribution of humid climate elements (Fe, Mn, Cr, V, Ni, and Co) and arid climate elements (Ca, Mg, K, Na, Sr, and Ba) have a close association with paleoclimate. Therefore, the C.I value (ratio of these representative elements) can be used to indicate the humidity of the paleoclimate (Moradi et al., 2016; Li et al., 2019; Awan et al., 2020). C.I is calculated by using the following formula (Awan et al., 2020):

$$C.I = \Sigma\,(Fe + Mn + Cr + V + Ni + Co)/\Sigma\,(Ca + Mg + K + Sr + Ba)$$

where C.I is the climatic index also known as C-value. C.I value <0.2 represents arid climate, while the standard C.I values for semi-arid, semiarid-humid, semi-humid, and humid climates are 0.2–0.4, 0.4–0.6, 0.6–0.8, and > 0.8, respectively (Ding et al., 2018; Awan et al., 2020). A slightly decreasing trend of C.I from top to bottom of the study interval has been observed (Fig. 11). The C.I value of the studied samples

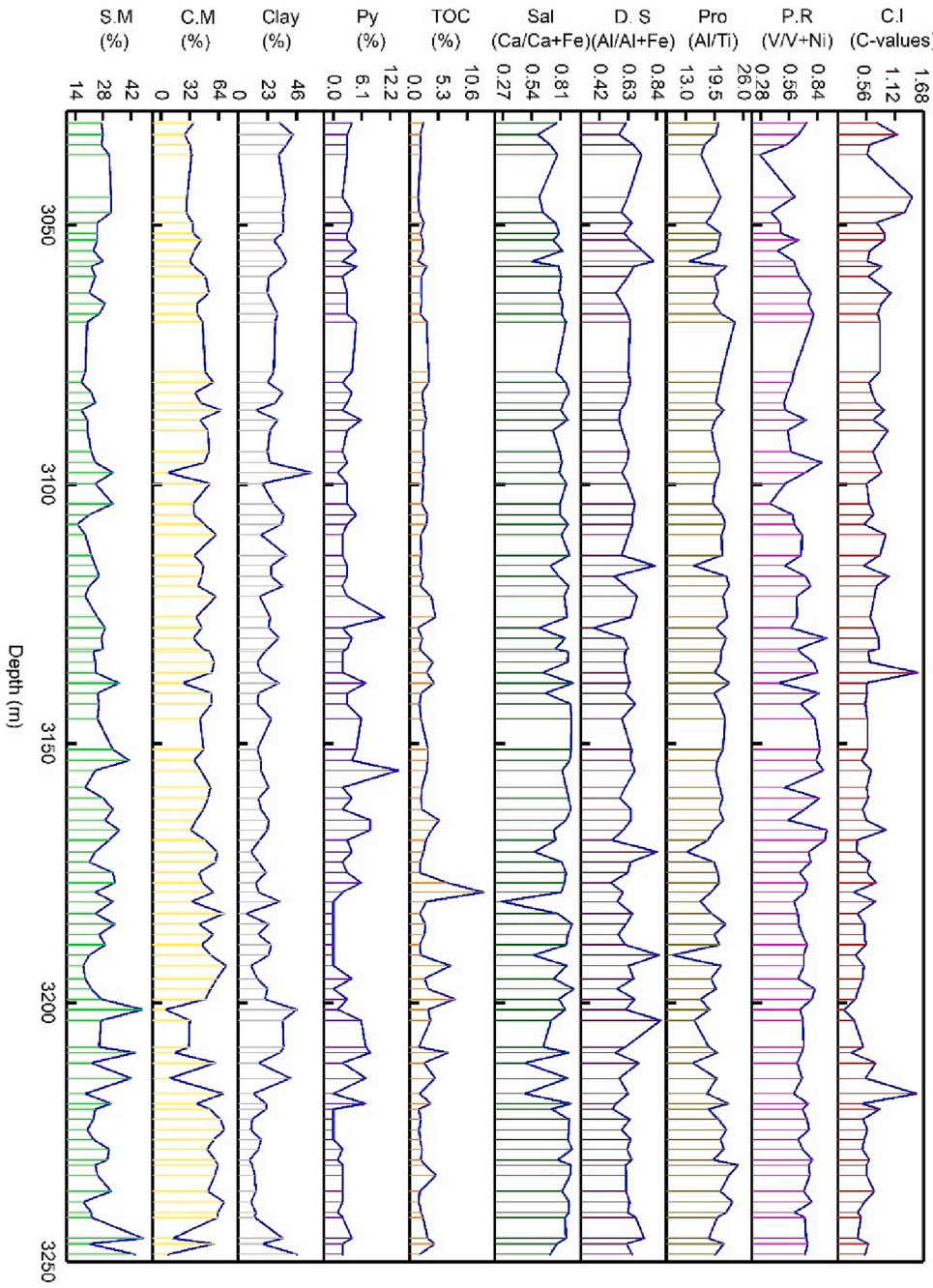

Fig. 13. Line plot showing the effect of different minerals composition and different geochemical parameters on the evolution of sedimentary setting during the deposition of the Es_3^L shale. A relatively higher amount of siliceous and clay minerals marked a fair amount of terrigenous influx during this phase. Anoxic conditions coupled with brackish to saline water prevailed during this phase. **Note:** S.M = siliceous minerals, C.M = carbonate minerals, Py = pyrite, Sal = salinity, D·S = detrital source, Pro = provenance, P.R = paleoredox, Cl = climate.

is ranging from 0.1 to 2.27 with an average value of 0.60. The average C. I value (C.*I* = 0.6) reflects semi-humid to humid climatic conditions during the deposition of the Es_3^L–Es_4^U shale in the study area (Fig. 11). Additionally, the chemical index of alteration (C.I.A) can give information concerning the intensity of subaerial weathering, ultimately providing information about the prevailing climatic conditions (Nesbitt and Young, 1982; Bahlburg, 2009; Wang et al., 2020). According to their interpretations, C.I.A values <0.7 correspond to cold and arid climatic conditions, C.I.A values of 0.7–0.8 indicate temperate climate, and C.I.A values of 0.8–1.0 reflect the hot and humid climatic conditions (Fig. 11). The formula to calculate these values is as follows (Nesbitt and Young, 1982):

$$C.I.A = Al/(Al + Na + K)$$

The trend of C.I.A values is also slightly decreasing from top to bottom of the study interval (Fig. 11). The average C.I.A value (0.73) of studied shale samples reflects the temperate climatic conditions. The results obtained from C.I.A values correspond to the results of C.I value. MSL has an average C.I value of 0.66 and C.I.A of 0.74, reflecting semi-humid and temperate climatic conditions (Table 2). The C.I values of CSL (avg. 0.64), LLL (avg. 0.53), ASL (avg. 0.49), DSL (avg. 0.53), SSL (avg. 0.83), and SDL (avg. 0.43) corresponding to semi-humid, semi-arid, semi-arid, semi-arid, humid, and semi-arid, respectively (Table 2). While the C.I.A values of CSL (avg. 0.74), LLL (avg. 0.73), ASL (avg. 0.75), DSL (avg. 0.70), SSL (avg. 0.71), and SDL (avg. 0.67) reflecting temperate, cold and arid climatic conditions (Table 2).

5.3. Detrital influx and provenance

Aluminum, titanium, silicon, and zirconium are frequently used to monitor the detrital influx due to their relatively immobile nature during the diagenetic processes (Algeo and Maynard, 2004; Maravelis et al.,

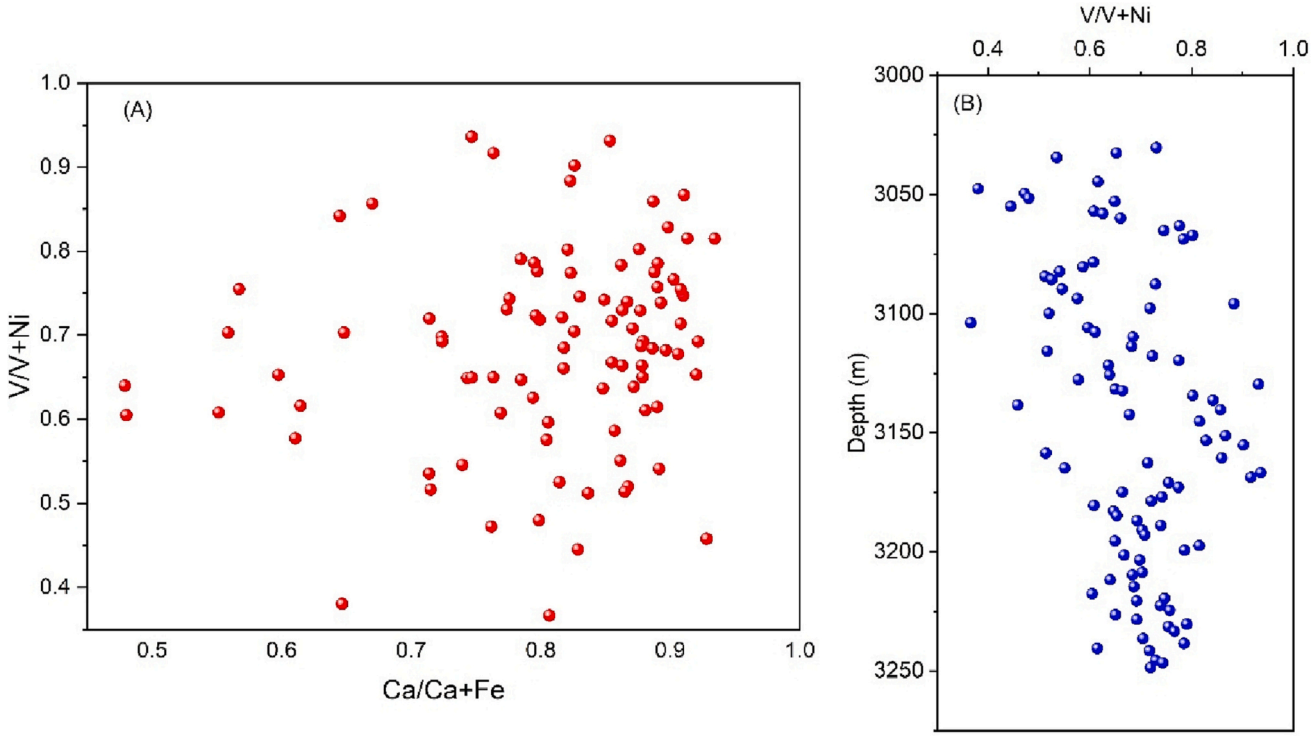

Fig. 14. (A) Shows the irregular relationship of paleoredox ($V/V + Ni$) conditions with salinity (Ca/Ca + Fe) of the Es_3^L shale in the study area. (B) Shows the positive relation of paleoredox conditions of the Es_3^L shale with burial depth in the study area.

Table 3
Organic geochemical parameters in the studied shale during the deposition of the Es_3^L shale.

Values range	TOC (%)	Tmax (°C)	S1 (mg/g)	S2 (mg/g)	HI (mg/g TOC)	PI (mg/g TOC)	Ro (%) (Jarvei)
Minimum	1.64	442	1.88	6.68	2.661	0.081	0.796
Maximum	8.83	454	4.11	41.22	16.422	0.318	1.012
Average	2.761	446.795	2.758776	12.86837	5.126	0.201	0.882327

2020). The Ti/Al is the most reliable geochemical proxy to reflect the intensity of detrital influx (Murphy et al., 2000). Titanium (Ti) is mostly contained in rutile (TiO_2) and ilmenite ($FeTiO_3$) minerals, while aluminum (Al) can be found in feldspars, clay, and other aluminum silicate minerals (Rimmer et al., 2004). The Ti/Al values range from 0.02 to 0.11 (avg. 0.05), corresponding to the restricted detrital influx in the study area (Fig. 11). Therefore, it can also be suggested that there was a very low detrital influx during the deposition of the Es_3^L–Es_4^U shale (Fig. 11), and also the OM preservation experienced very little influence of detrital influx dilution. This interpretation also indicated that the higher TOC contents in the Es_3^L–Es_4^U shale are not a product associated with the detrital influx (Fig. 12A). While, the ratios of Al/Al + Fe (avg. 0.61) show a terrestrial source because Al/Al + Fe ratio >0.4 indicates a terrestrial source (Liu et al., 2015, Fig. 11), and this interpretation is also consistent with the results derived from the Ti/Al ratios in the studied shale samples. In addition, Al/Ti ratios can be utilized to interpret the provenance because their values in sedimentary rocks have a very close association with parent rocks. Hence, the Al/Ti values >21 indicate felsic igneous rocks, values between 8 and 21 show intermediate igneous rocks, and values <8 reflect mafic igneous rocks (Moradi et al., 2016). The Al/Ti ratios range from 8.38 to 41.6 (avg. 20.1) (Fig. 11). These results indicate that the debris may be derivative of intermediate igneous rocks in the studied shale samples.

Ti/Al and Al/Al + Fe ratios of all lithofacies in the study area show a restricted detrital influx during the deposition of studied shale in the Boxing, Dongying Depression (Table 2). While Al/Ti ratios for all lithofacies indicate that the sediments may be derivative of intermediate igneous rocks except SDL (debris may have resulted from felsic igneous rocks for this lithofacies) (Table 2).

5.4. Paleoredox conditions and water depth

The redox conditions play an important part in OM deposition, accumulation, and preservation. Redox-sensitive elements i.e., V, Ni, and Co, are used to predict the paleoredox conditions in this study (Lewan, 1984; Tribovillard et al., 2006; Yin et al., 2018). Vanadium can be concentrated under a reducing environment while nickel can easily be enriched under oxidizing conditions, therefore paleoredox conditions of the water column can be predicted by $V/V + Ni$ ratios in sediments (Jones and Manning, 1994; Mongenot et al., 1996; Rimmer et al., 2004). V/V + Ni value >0.82 indicates euxinic conditions, ratios between 0.54 and 0.8 indicates anoxic, 0.46–0.6 show dysoxic conditions, and <0.46 shows oxic environments (Jones and Manning, 1994; Li et al., 2011). The V/V + Ni ratios are ranging from 0.23 to 0.99 with an average of 0.74, corresponding to anoxic conditions during the deposition of the $Es3^L$–$Es4^U$ shale in the study area (Fig. 11). Furthermore, the results obtained from the cross-plot of V/V + Ni and Ni/Co are parallel with the interpretations derived from V/V + Ni ratios. This cross plot also indicates the dysoxic to anoxic conditions during the deposition of the studied shale (Fig. 12B). These interpretations indicate that all the lithofacies of the Es_3^L–Es_4^U shale were deposited in an anoxic except SDL which was deposited in a euxinic environment (Table 2).

In addition, ratios of Fe/Ca + Mg were used to discriminate the water depth during the deposition of the Es_3^L–Es_4^U shale (Fig. 11). Ca and Mg are

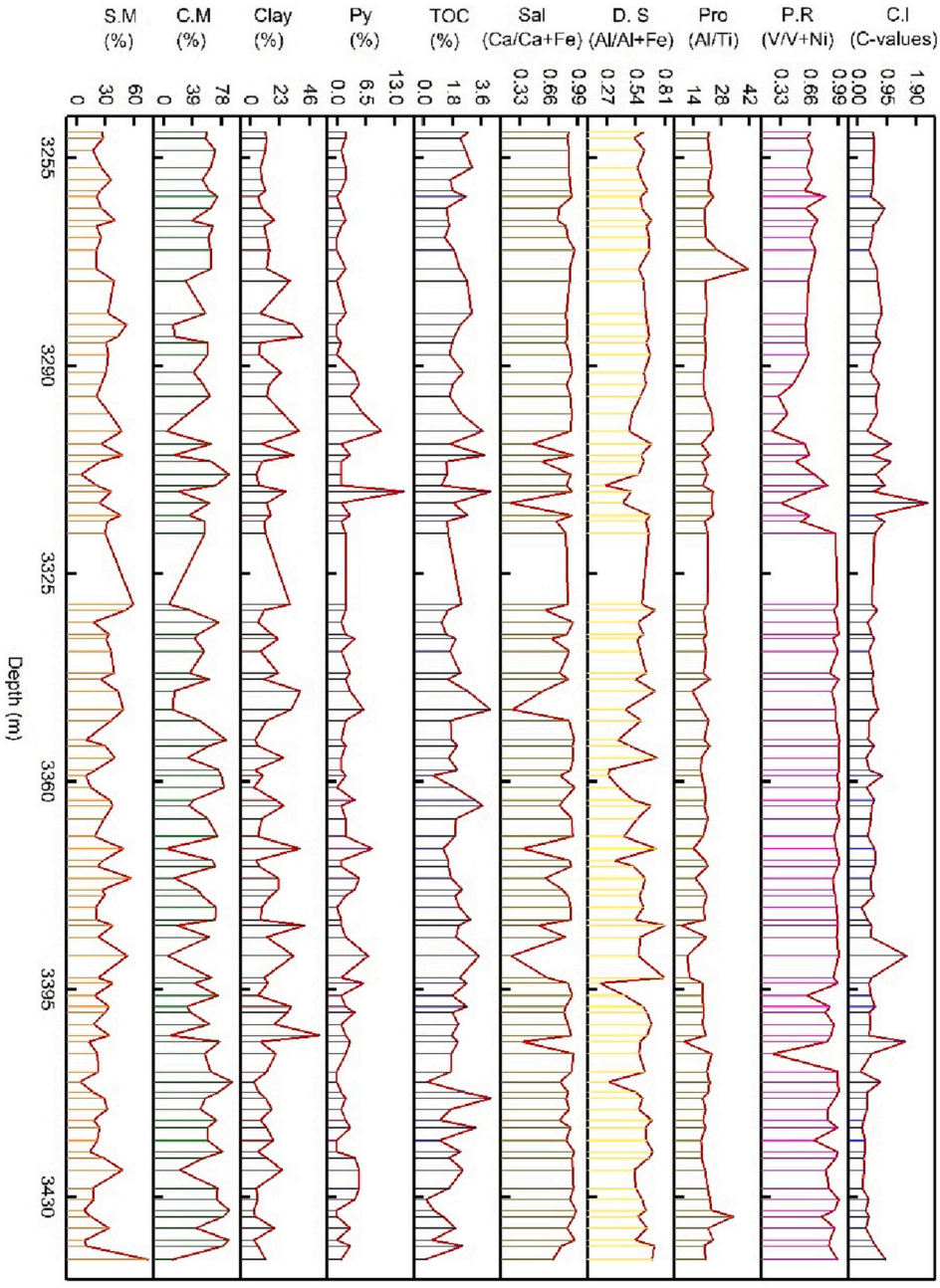

Fig. 15. Line plot showing the effect of different minerals composition and different geochemical parameters on the evolution of sedimentary setting during the deposition of the Es_4^U shale. A low amount of siliceous and clay minerals marked the restricted terrigenous influx during this phase. Anoxic conditions coupled with saline water prevailed during this phase. Semiarid-humid climatic conditions support the deposition of carbonate minerals which can be confirmed by the higher concentration of carbonate minerals in the figure. **Note:** S.M = siliceous minerals, C.M = carbonate minerals, Py = pyrite, Sal = salinity, D·S = detrital source, Pro = provenance, P.R = paleoredox, C.I = climate.

Table 4
Organic geochemical parameters in the studied shale during the deposition of the Es_4^U shale.

Values range	TOC (%)	Tmax (∘C)	S1 (mg/g)	S2 (mg/g)	HI (mg/g TOC)	PI (mg/g TOC)	Ro (%) (Jarvei)
Minimum	0.52	425	1.02	2.53	1.007	0.140	0.49
Maximum	3.35	454	5.36	13.64	5.434	0.389	1.012
Average	2.083421	446.8158	2.782632	7.235263	2.882	0.278	0.88268

primarily concentrated in carbonate and mudrocks in deep water, while Fe is mainly enriched in terrigenous clastic rocks (Restituito, E. 1987; Chen et al., 2016). The higher Fe/Ca + Mg ratios indicate deep water conditions during the deposition (Fig. 11). The Fe/Ca + Mg values range from 0.02 to 2.45 with an average value of 0.25 in the study area. Fe/Ca + Mg ratio in the MSL ranges from 0.04 to 0.58 (avg. 0.25), corresponding to moderate water during its deposition (Table 2). The Fe/Ca + Mg ratios in the CSL (avg. 0.24), LLL (avg. 0.24), ASL (avg. 0.13), and DSL (avg. 0.15) also correspond to shallow water depth during their deposition (Table 2). While the ratios in the SSL (avg. 0.67) indicate deep water conditions and the ratios in the SDL (avg. 0.09) show shallow water depth during their deposition in the Boxing Sag, Dongying Depression (Table 2).

5.5. Interpretation of sedimentary environment

The sedimentary environment of the study area has been constructed based on the interpretations of sedimentary structures, mineral

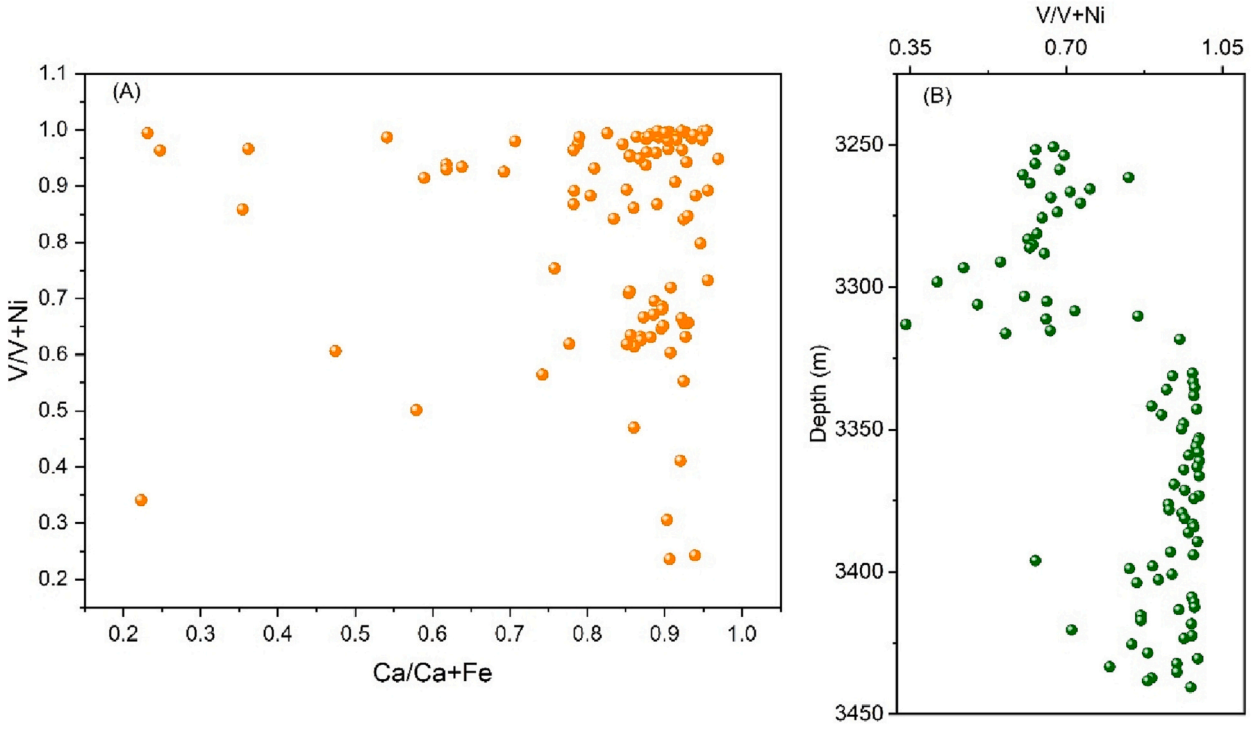

Fig. 16. (A) Shows the irregular relationship of paleoredox ($V/V + Ni$) conditions with salinity (Ca/Ca + Fe) of the Es_4^U shale in the study area. (B) Shows the positive relation of paleoredox conditions of the Es_4^U shale with burial depth in the study area.

composition, and various geochemical proxies. The detailed interpretation of the sedimentary environment allows us to distinguish two major phases in the evolution of the sedimentary environment during the Paleogene in Boxing Sag, Jiyang Sub-basin.

5.5.1. Variations of the sedimentary environment during the deposition of the Es_3^L shale

This phase is characterized by abundant terrigenous input in shallow to deep open lacustrine environment (Fig. 13 & 17A). The terrigenous material is originated from eroded bedrocks around the lacustrine basin and is transported by freshwater input or wind flow (Kong et al., 2022). The source of detrital influx is terrestrial as suggested by Al/Al + Fe geochemical proxy (avg. 0.62) (Fig. 14). The sediment debris is derived from intermediate igneous source rocks which are suggested by Al/Ti (avg. 19.86) ratios (Fig. 13). Semi-humid climatic conditions prevailed during this phase which is marked by the C-values (avg. 0.66) (Fig. 13). The formation of a reducing environment is considered to be promoted by the increase in salinity (Kong et al., 2022). In our study area, paleoredox conditions have no obvious relationship with salinity but have a positive relationship with water depth (Fig. 14A–B). Therefore, it can be suggested that the main reason for increasing the reducing conditions in the ancient lake water column was the increase of water depth rather than salinity. Strong oxic conditions prevailed in a shallower part of the lake, corresponding to the less saline water. While dysoxic and anoxic zones are characterized by saline and hypersaline water conditions, respectively (Fig. 17A). Euxinic conditions are marked by the highest sulfur content coupled with anoxic conditions and the distribution of pyrite (Khan et al., 2021). It is demonstrated by high bio productivity, corresponding to the higher preservation of OM in the sediments and higher TOC contents (avg. 3.06 wt%) (Fig. 17A, Table 3). Type-I kerogen is present in this shale (Fig. 6), which corresponds to the algal bloom during this phase of deposition. Bio productivity bloom is due to the higher precipitation rate during this phase (Fig. 17A). Below the wave base, the terrigenous sediments are transported by turbidity currents. The suspension settling of fine-grain material and biogenic remains also occurred below the wave base zone in the dysoxic lake water. Calcium ions (Ca^+) are continuously supplied to this small basin from the surrounding Cambrian-Ordovician carbonate bedrocks (Li et al., 2020; Khan et al., 2022a, Fig. 17A). These interpretations are consistent with other authors (Liang et al., 2017, 2018; Bai et al., 2020).

5.5.2. Variations of the sedimentary environment during the deposition of the Es_4^U shale

This phase is marked by relatively limited terrigenous input in shallow to semi-deep open lacustrine environments (Fig. 15 & 17B). It is demonstrated by low bio productivity, corresponding to the lower preservation of OM in the sediments and low TOC contents (avg. 2.01 wt %) (Fig. 17B, Table 4). Bio productivity decline is due to the higher evaporation rate during the deposition of shale (Fig. 17B). Strong evaporation conditions prevailed, corresponding to the higher salinity (Fig. 17B). The strong saline water conditions are also marked by Ca/Ca + Fe ratios (avg. 0.82) (Fig. 15, Table 4). During the deposition of the Es_4^U shale, the reducing conditions also have no clear connection with salinity but good relation with increasing water depth in the study area (Fig. 16A–B). In this case, the water depth also played an important role to enhance the reducing conditions. The concentration of clay and siliceous minerals during this phase was relatively low due to restricted terrigenous input and lack of freshwater inflow (Fig. 15 & 17B). Semiarid-humid climatic conditions prevailed during this period of deposition (Fig. 15). These climatic conditions are consistent with the higher concentration of carbonate minerals (avg. 52.9 %) because these conditions support the deposition of carbonate minerals (Fig. 15). The interpretations deduced from these analyses are also consistent with previous literature (Liang et al., 2017, 2018; Bai et al., 2020).

Based on several shreds of evidence deduced from various qualitative and quantitative analyses, our model suggests that non-laminated calcareous shale, mixed and siliceous shale were deposited in model A (Es_3^L shale) due to higher rainfall and abundant freshwater, and terrigenous influx. In the deeper part, the formation of pyrite also took place due to higher sulfur content and organic matter. The abundance of OM was due to the higher primary bio productivity. The laminated shale intervals also developed in the deeper due to a lack of biogenic activity

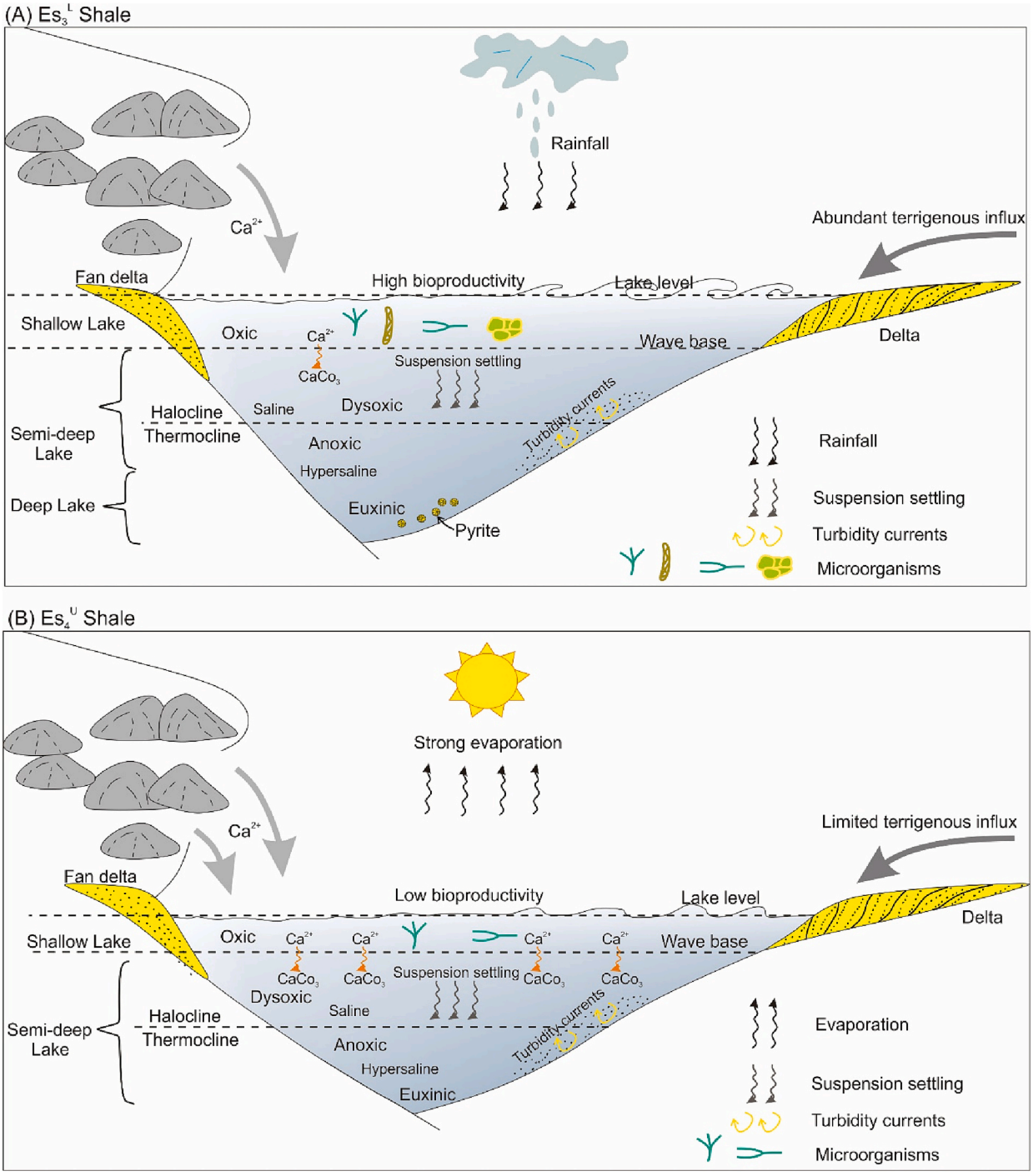

Fig. 17. Sedimentary evolution model of the Es_3^L–Es_4^U shale of the Shahejie Formation in FY1 well in the Boxing Sag, Dongying Depression (Bohai Bay Basin). (A) Model showing the semi-humid climatic conditions with the sufficient terrigenous influx and rainfall during the deposition of the Es_3^L shale. (B) Model showing the semiarid-humid climate with limited terrigenous input and strong evaporation during the deposition of the Es_4^U shale.

(bioturbation). On the other hand, strong evaporation supported the formation of dolomite, limestone, and anhydrite in the Es_4^U shale. Due to low bio productivity, bioturbation was absent which supported the formation and preservation of laminations due to the absence of in-place biota. So, the laminated shale developed during this phase of deposition. And due to limited terrigenous supply, the siliceous rocks were sparsely deposited during this phase of deposition. This study provides information regarding the distribution of various minerals, TOC content, R_o, lithofacies, and their depositional environment. Based on these discussions, it is very easy to choose a favorable horizon for shale oil and gas exploration in a lacustrine environment.

6. Conclusions

In this study, a geochemical record of variation and fluctuation in the sedimentary environment of the lacustrine basin is analyzed based on extensive shale samples collected from the Es_3^L–Es_4^U shale of the Paleogene Shahejie Formation of the FY1 well in the Boxing Sag, Dongying Depression.

Different geochemical proxies including Sr/Ba, Ca/Ca + Fe, C.I

value, C.I.A values, Ti/Al, Al/Al + Fe, Al/Ti, V/V + Ni, Ni/Co, and Fe/Ca + Mg were used to interpreting salinity, paleoclimate, detrital influx, provenance, paleoredox, and water depth of the depositional environment in the studied shale. The detailed interpretation of the sedimentary environment suggests that during the deposition of Es_3^L shale, the terrigenous influx was high in shallow to a deep open lacustrine system with higher primary biogenic productivity. Semi-humid climatic conditions with higher precipitation rates prevailed during the deposition of this shale. On the other hand, relatively limited terrigenous input with low bioproductivity prevailed during the deposition of Es_4^U shale in the study area. Semiarid to humid climatic conditions with strong evaporation prevailed during the deposition of this shale.

After detailed analysis, it can be speculated that the main reason for the enhancement of reducing conditions in the lake water column in the study area was the increase of water depth rather than salinity. This study provides information regarding the distribution of various minerals, TOC content, R_o, lithofacies, and their depositional environment. Based on these discussions, it is very easy to choose a favorable horizon for shale oil and gas exploration in a lacustrine environment.

Supplementary data to this article can be found online at https://doi.org/10.1016/j.chemer.2023.125978.

CRediT authorship contribution statement

Danish Khan: Conceptualization, writing - original draft, Writing - review & editing. Liu Zijun & Longwei Qiu: Methodology, Writing - review & editing. Liu Kuiyuan, Yang Yongqiang, Nie Cong, & Liu Bin: Data curation, Methodology, Review, & Editing. Xin Li & Yerejiepu Habulashenmu: Software, Field Study.

Declaration of competing interest

The authors declare that they have no known competing financial interests or personal relationships that could have appeared to influence the work reported in this paper.

Acknowledgments

This research work was supported by the National Natural Science Foundation of China (Nos. 41972099), and the project of “Jiyang Depression Continental Faulted Lacustrine Basin Shale Oil National Demonstration Zone”. The authors would like to thank Shengli Oil Company Dongying for providing core samples and other necessary geological data from FY1 well for this research work. The authors would also like to acknowledge the School of Geosciences, China University of Petroleum East China for analytical support and financial sustenance.

References

Abouelresh, M.O., Slatt, R.M., 2012. Lithofacies and sequence stratigraphy of the Barnett Shale in east-central Fort Worth Basin, Texas. AAPG Bull. 96, 1–22.
Algeo, T.J., Maynard, J.B., 2004. Trace-element behavior and redox facies in core shales of upper pennsylvanian Kansas-type cyclothems. Chem. Geol. 206 (3), 289–318.
Aplin, A.C., Macquaker, J.H., 2011. Mudstone diversity: origin and implications for source, seal, and reservoir properties in petroleum systems. AAPG Bull. 95, 2031–2059.
Awan, R.S., Liu, C., Gong, H., Dun, C., Tong, C., Chamssidini, L.G., 2020. Paleo-sedimentary environment in relation to enrichment of organic matter of early cambrian black rocks of niutitang formation from xiangxi area China. Mar. Petrol. Geol. 112, 104057.
Bahlburg, H., 2009. A review of the Chemical Index of Alteration (CIA) and its application to the study of Neoproterozoic glacial deposits and climate transitions. In: Arnaud, E., Halverson, G.P., Shields, G.A. (Eds.), The Geological Record of Neoproterozoic Glaciations, 36. Geological Society of London, Memoir, pp. 81–91.
Bai, C., Yu, B., Han, S., Shen, Z., 2020. Characterization of lithofacies in shale oil reservoirs of a lacustrine basin in eastern China: implications for oil accumulation. J. Pet. Sci. Eng. 195, 107907.
Bechtel, A., Jia, J., Strobl, S.A.I., Sachsenhofer, R.F., Liu, Z., Gratzer, R., Püttmann, W., 2012. Paleoenvironmental conditions during deposition of the upper cretaceous oil shale sequences in the Songliao Basin (NE China): implications from geochemical analysis. Org. Geochem. 46, 76–95.
Bohacs, K.M., Carroll, A.R., Neal, J.E., Mankiewicz, P.J., 2000. Lake-basin type, source potential, and hydrocarbon character: an integrated sequence-stratigraphic-geochemical framework. In: Gierlowski-Kordesch, E.H., Kelts, K.R. (Eds.), Lake Basins Through Space and Time, 46. AAPG Studies in Geology, pp. 3–34.
Boström, K., Kraemer, T., Gartner, S., 1973. Provenance and accumulation rates of opaline silica, Al, ti, fe, mn, cu, ni and co in Pacific pelagic sediments. Chem. Geol. 11, 123–148.
Bruner, K.R., Walker-Milani, M., Smosna, R., 2015. Lithofacies of the Devonian Marcellus Shale in the Eastern Appalachian Basin, USA. J. Sediment. Res. 85, 937–954.
Carroll, A.R., Bohacs, K.M., 2001. Lake-type controls on petroleum source rock potential in nonmarine basins. AAPG Bull. 85, 1033–1053.
Chen, Z., Huang, W., Liu, Q., Linye, Z., Zhang, S., 2016. Geochemical characteristics of the paleogene shales in the Dongying depression, eastern China. Mar. Petrol. Geol. 73, 249–270.
Cichon-Pupienis, A.K., Littke, R., Lazauskienė, J., Baniasad, A., Pupienis, D., Radzevičius, S., Siliauskas, L., 2021. Geochemical and sedimentary facies study – implication for driving mechanisms of organic matter enrichment in the lower Silurian fine-grained mudstones in the Baltic Basin (W Lithuania). Int. J. Coal. Geol. 244, 103815.
Deng, H.W., Qian, K., 1993. In: Sedimentary Geochemistry and Environment Analysis. Gansu Technology Publishing House, Lanzhou, pp. 1–150.
Ding, J., Zhang, J., Tang, X., Huo, Z., Han, S., Lang, Y., Zheng, Y., Li, X., Liu, T., 2018. Elemental geochemical evidence for depositional conditions and organic matter enrichment of Black Rock Series Strata in an Inter-Platform Basin: the Lower Carboniferous Datang Formation, Southern Guizhou, Southwest China. Minerals 8 (11), 509.
Gonçalves, F.T., 2002. Organic and isotope geochemistry of the early cretaceous rift sequence in the Camamu Basin, Brazil: paleolimnological inferences and source rock models. Org. Geochem. 33, 67–80.
Green, H., Šegvić, B., Zanoni, G., Omodeo-Salé, S., Adatte, T., 2020. Evaluation of shale source rocks and clay mineral diagenesis in the Permian Basin, USA: inferences on basin thermal maturity and source rock potential. Geosciences 10 (10), 381.
Hao, F., Zhou, X., Zhu, Y., Yang, Y., 2011. Lacustrine source rock deposition in response to co-evolution of environments and organisms controlled by tectonic subsidence and climate, Bohai Bay Basin, China. Org. Geochem. 42 (4), 323–339. https://doi.org/10.1016/j.orggeochem.2011.01.010.
Hammes, U., Frébourg, G., 2012. Haynesville and Bossiermudrocks: a facies and sequence stratigraphic investigation, East Texas and Louisiana, USA. Mar. Pet. Geol. 31, 8–26.
Hosterman, J.W., Whitlow, S.I., 1980. Munsell Color Value as Related to Organic Carbon in Devonian Shale of the Appalachian Basin. USGS Open-File Report 80-660. U.S. Geological Survey, Reston, VA.
Hu, X.F., Liu, Z.J., Liu, R., et al., 2012a. Clay mineral and inorganic geochemical characteristics of Eocene Huadian formation in Huadian Basin and their paleoenvironment implications. J. China Coal Soc. 37 (3), 416–423 (in Chinese with English Abstract).
Huang, C., Wang, H., Wu, Y., Wang, J., Chen, S., Ren, P., Liao, Y., Zhao, S., Xia, C., 2012. Genetic types and sequence stratigraphy models of palaeogene slope break belts in qikou sag, Huanghua depression, Bohai Bay basin, eastern China. Sediment. Geol. 261, 65–75. https://doi.org/10.1016/j.sedgeo.2012.03.005.
Jarvie, D.M., 2012. Shale resource systems for oil and gas: part 2—shale-oil resource systems. In: Breyer, J.A. (Ed.), Shale Reservoirs—Giant Resources for the 21st Century, 97. AAPG Memoir, pp. 89–119.
Jarvie, D.M., Hill, R.J., Ruble, T.E., Pollastro, R.M., 2007. Unconventional shale-gas systems: the mississippian Barnett shale of north-Central Texas as one model for thermogenic shale-gas assessment. AAPG Bull. 91, 475–499. https://doi.org/10.1306/12190606068.
Jia, J., Bechtel, A., Liu, Z., Strobl, S.A., Sun, P., Sachsenhofer, R.F., 2013. Oil shale formation in the upper cretaceous nenjiang formation of the Songliao Basin (NE China): implications from organic and inorganic geochemical analyses. Int. J. Coal Geol. 113, 11–26.
Jiang, Z., Liu, H., Zhang, S., Su, X., Jiang, Z., 2011. Sedimentary characteristics of large-scale lacustrine beach-bars and their formation in the eocene boxing sag of Bohai Bay basin, East China. Sedimentology 58, 1087–1112.
Jones, B.J., Manning, A.C., 1994. Comparison of geochemical indices used for the interpretation of palaeoredox conditions in ancient mudstones. Chem. Geol. 11 (11), 111–129.
Katz, B., Lin, F., 2014. Lacustrine basin unconventional resource plays: key differences. Mar. Pet. Geol. 56, 255–265.
Khan, D., Qiu, L., Liang, C., Mirza, K., Rehman, S.U., Han, Y., Hannan, A., Kashif, M., Kra, K.L., 2021. Genesis and distribution of pyrite in the lacustrine shale: evidence from the Es3x shale of the Eocene Shahejie Formation, Zhanhua Sag, East China. ACS Omega 7 (1), 1244–1258.
Khan, D., Qiu, L., Liang, C., Martizzi, P., Mirza, K., Liu, J., 2022a. Tracing forming mechanism of the sparry calcite growth in the lacustrine shale of East China: a glimpse into the role of organic matter in calcite transformation. Geol. J. 57 (5), 1–17.
Khan, D., Liang, C., Qiu, L., Mirza, K., Wang, Y., Kashif, M., Rehman, S.U., Wang, Y., Teng, J., 2022b. Depositional environment and lithofacies analyses of the eocene lacustrine shale in the Bohai Bay basin: insights from mineralogy and elemental geochemistry. Acta Geol. Sin. Engl. Ed. https://doi.org/10.1111/1755-6724.14985.
Kong, X., Jiang, Z., Ju, B., Liang, C., Cai, Y., Wu, S., 2022. Fine-grained carbonate formation and organic matter enrichment in an Eocene saline rift lake (Qianjiang Depression): constraints from depositional environment and material source. Mar. Pet. Geol. 138, 105534.

Könitzer, S.F., Davies, S.J., Stephenson, M.H., Leng, M.J., 2014. Depositional controls on mudstone lithofacies in a basinal setting: implications for the delivery of sedimentary organic matter. J. Sediment. Res. 84, 198–214.
Lan, X.H., Ma, D.X., Xu, M.G., et al., 1987. Some geochemical signs and their importance for sedimentary facies. Mar. Geol. Quat. Geol. 7 (1), 39 (in Chinese with English Abstract).
Lewan, M.D., 1984. Factors controlling the proportionality of vanadium to nickel in crude oils. Geochim. Cosmochim. Acta 48 (11), 2231–2238.
Li, N., Hu, C.Y., Ma, Z.W., 2011. Main control factors of high quality hydrocarbon source rocks of the Upper Permian Dalong Formation at Shangsi Section of Guangyuan, Sichuan Province. Palaeogeography 13 (3), 347–353 (in Chinese with English Abstract).
Li, C., Zhu, X., Zhu, S., Geng, M., Bi, Y., Shu, Q., Xu, F., 2015. Shale reservoir characteristics of the lower 3rd member of Shahejie Formation, Luojia Area, Zhanhua Sag. Acta Sedimentol. Sin. 33, 795–808.
Li, L., Liu, Z., George, S., Sun, P., Xu, Y., Meng, Q., Wang, K., Wang, J., 2019. Lake evolution and its influence on the formation of oil shales in the Middle Jurassic Shimengou Formation in the Tuanyushan area, Qaidam Basin, NW China. Geochemistry 79 (1), 162–177.
Li, Q., You, X., Jiang, Z., Wu, S., Zhang, R., 2020. The origins of carbonate minerals of a source-controlled lacustrine carbonate succession in the shulu sag, Bohai Bay basin: implications for porosity development and paleoenvironment. Mar. Pet. Geol. 122, 104673.
Liang, C., Cao, Y., Jiang, Z., Wu, J., Guo-qi, S., Wang, Y., 2017. Shale oil potential of lacustrine black shale in the eocene Dongying depression: implications for geochemistry and reservoir characteristics. AAPG Bull. 101, 1835–1858.
Liang, C., Jiang, Z., Cao, Y., Wu, J., Wang, Y., Hao, F., 2018. Sedimentary characteristics and origin of lacustrine organic-rich shales in the salinized eocene Dongying depression. Bull. Geol. Soc. Am. 130, 154–174.
Liu, B.J., 1980. In: Sedimentary Petrology. Geological Publishing House, Beijing, pp. 286–289.
Liu, B., Bechtel, A., Sachsenhofer, R.F., Gross, D., Grazter, R., Chen, X., 2017. Depositional environment of oil shale within the second member of permian lucaogou formation in the santanghu basin, Northwest China. Int. J. Coal Geol. 175, 10–25.
Liu, Z.H., Zhuang, X.G., Teng, G.E., Xie, X.M., Yin, L.M., Bian, L.Z., Feng, Q., Algeo, T., 2015. The lower cambrian niutitang formation at yangtiao (Guizhou, SW China): organic matter enrichment, source rock potential, and hydrothermal influences. J. Pet. Geol. 38, 411–432.
Loucks, R.G., Ruppel, S.C., 2007. Mississippian Barnett Shale: Lithofacies and depositional setting of a deep-water shale-gas succession in the Fort Worth Basin, Texas. AAPG Bull. 91, 579–601.
Ma, Y., Lu, Y., Liu, X., Zhai, G., Wang, Y., Zhang, C., 2019. Depositional environment and organic matter enrichment of the lower Cambrian Niutitang shale in western Hubei Province, South China. Mar. Pet. Geol. 119, 381–393.
Ma, Y., Fan, M., Lu, Y., Liu, H., Hao, Y., Xie, Z., Peng, L., Du, X., Hu, H., 2017. Middle eocene paleohydrology of the Dongying depression in eastern China from sedimentological and geochemical signatures of lacustrine mudstone. Palaeogeogr. Palaeoclimatol. Palaeoecol. 479, 16–33.
Maravelis, A.G., Offler, R., Pantopoulos, G., Collins, W.J., 2020. Provenance and tectonic setting of the early permian sedimentary succession in the southern edge of the Sydney Basin, eastern Australia. Geol. J. 56, 2258–2276.
Martel, T., 2013. Pitfalls in assessing lacustrine shale versus marine shale prospects. In: Oral Presentation Given at AAPG 2013 Annual Convention and Exhibition, Pittsburgh, Pennsylvania, May 19–22, 2013.
Mongenot, T., Tribovillard, N.P., Desprairies, A., Lallier-Vergès, E., Laggoun-Defarge, F., 1996. Trace elements as palaeoenvironmental markers in strongly mature hydrocarbon source rocks, the cretaceous La Luna formation of Venezuela. Sediment. Geol. 103 (1), 23–37.
Moradi, A.V., Sari, A., Akkaya, P., 2016. Geochemistry of the miocene oil shale (Hanili Formation) in the ankr-orum basin, Central Turkey: implications for paleoclimate conditions, source–area weathering, provenance and tectonic setting. Sediment. Geol. 34 (15), 289–303.
Murphy, A.E., Sageman, B.B., Hollander, D.J., Lyons, T.W., Brett, C.E., 2000. Black shale deposition and faunal overturn in the devonian appalachian basin: clastic starvation, seasonal water-column mixing, and efficient biolimiting nutrient recycling. Paleoceanography 15 (3), 280–291. https://doi.org/10.1029/1999PA000445.
Nesbitt, H.W., Young, G.M., 1982. Early proterozoic climates and plate motions inferred from major element chemistry of lutites. Nature 299, 715–717.
Niu, X., Yan, D., Zhuang, X., Liu, Z., Li, B., Wei, X., Xu, H., Li, D., 2018. Origin of quartz in the lower cambrian niutitang formation in South Hubei province, upper Yangtze platform. Mar. Pet. Geol. 96, 271–287.
Peters, K., 1986. Guidelines for evaluating petroleum source rock using programmed pyrolysis. AAPG Bull. 70 (3), 318–329.
Restituito, E., 1987. Consequences of redox conditions on the distribution of cations in a meromictic oligotrophic Lake. Hydrobiologia 144, 63–75. https://doi.org/10.1007/BF00008052.
Rimmer, S.M., Thompson, J.A., Goodnight, S.A., Robl, T.L., 2004. Multiple controls on the preservation of organic matter in devonian mississippian marine black shales: geochemical and petrographic evidence. Palaeogeogr. Palaeoclimatol. Palaeoecol. 215, 125–154.
Scheeder, G., Weniger, P., Blumenberg, M., 2020. Geochemical implications from direct Rock-Eval pyrolysis of petroleum. Org. Geochem. 146, 104051.
Si, X.Q., Zhang, J.L., 2008. Mechanism of secondary pore of the beach bar sandstones in the upper Es4 of the Palaeogene, Boxing Sag. Geol. Sci. Technol. Inform. 27 (1), 59–63.
Tao, S., Xu, Y.B., Tang, D.Z., et al., 2017. Geochemistry of the shitoumei oil shale in the Santanghu Basin, Northwest China: implications for paleoclimate conditions, weathering, provenance and tectonic setting. Int. J. Coal Geol. 18, 42–56.
Tribovillard, N., Algeo, T.J., Lyons, T., Riboulleau, A., 2006. Trace metals as paleoredox and paleoproductivity proxies: an update. Chem. Geol. 232, 12–32.
Wang, G.M., 2012. Laminae combination and genetic classification of Eogene shale in Jiyang Depression. J. Jilin Univ. (Earth Sci. Ed.) 42 (3), 666–680.
Wang, P., Du, Y., Yu, W., Algeo, T.J., Zhou, Q., Xu, Y., Qi, L., Yuan, L., Pan, W., 2020. The chemical index of alteration (CIA) as a proxy for climate change during glacial-interglacial transitions in earth history. Earth Sci. Rev. 201, 103032.
Wei, W., Algeo, T.J., 2019. Elemental proxies for paleosalinity analysis of ancient shales and mudrocks. Geochem. Cosmochim. Acta. https://doi.org/10.1016/j.gca.2019.06.034.
Xie, X., Li, M., Littke, R., Huang, Z., Ma, X., Jiang, Q., Snowdon, L.R., 2016. Petrographic and geochemical characterization of microfacies in a lacustrine shale oil system in the Dongying sag, jiyang depression, Bohai Bay basin, eastern China. Int. J. Coal Geol. 165, 49–63.
Xue, Y., Wu, Z.P., Li, W., Nie, W.L., 2013. Cenozoic Basin structure in the Dongying depression and its control over reservoir. Geotecton. Metallog. 37 (2), 206–212.
Yin, J., Wang, Q., Hao, F., Guo, L., Zou, H., 2018. Palaeoenvironmental reconstruction of lacustrine source rocks in the lower1st member of the shahejie formation in the raoyang sag and the baxian sag, Bohai Bay basin, eastern China. Palaeogeogr. Palaeoclimatol. Palaeoecol. 495, 87–104.
Yuan, J., Jiang, Z.X., 2000. Synthetic model of sedimentation, diagenesis and pool formation of paleogene for Dongying sag. J. Mineral. Petrol. 20 (1), 57–60 (in Chinese with English abstract).
Zhang, K., Liu, R., Liu, Z., Li, B., Han, J., Zhao, K., 2020. Influence of volcanic and hydrothermal activity on organic matter enrichment in the Upper Triassic Yanchang Formation, southern Ordos Basin, Central China. Mar. Petrol. Geol. 112, 104059.
Zhu, X.M., Zhang, S.P., Han, X.F., et al., 2013. On the differences of reservoir quality of shahejie formation in steep slope zones of jiyang sag. Acta Sedimentol. Sin. 31 (6), 1094–1104 (in Chinese with English Abstract).